Molina Puerto, J.; Bonastre Cano, JA.; Fernández Sáez, J.; Del Río García, AI.; Cases Iborra, FJ. (2016). Electrochemical synthesis of polypyrrole doped with graphene oxide and its electrochemical characterization as membrane material. Synthetic Metals. 220:300-310. doi:10.1016/j.synthmet.2016.06.028.

Electrochemical synthesis of polypyrrole doped with graphene oxide and its electrochemical characterization as membrane material

J. Molina, J. Bonastre, J. Fernández, A.I. del Río, F. Cases*

Departamento de Ingeniería Textil y Papelera, EPS de Alcoy, Universitat Politècnica de València, Plaza Ferrándiz y Carbonell s/n, 03801 Alcoy, Spain

Abstract

Polypyrrole (PPy) doped with graphene oxide (GO) has been electrochemically obtained by potentiostatic synthesis and its electrochemical behavior as membrane material has been studied for the first time. Fourier transform infrared spectroscopy with attenuated total reflection showed the formation of the hybrid material due to presence of PPy and GO bands. Field emission scanning electron microscopy micrographs showed the effective incorporation of GO sheets and the formation of a 3-D porous material with high surface area. Scanning electrochemical microscopy of PPy/GO films showed positive feedback close to the ideal conducting behavior, indicating a good electroactivity. Electrochemical impedance spectroscopy (EIS) was employed to measure the electrochemical properties of the coatings by two-, three-, and four-electrode configurations. The electronic conductivity of PPy/GO film, measured between two metallic conductors, was $4.7 \cdot 10^{-6}$ S/cm. Its ionic conductivity was superior ($1.6 \cdot 10^{-3}$ S/cm) due to the high porosity of the material as demonstrated by cyclic voltammetry and EIS measurements, where the PPy/GO film was employed as a free-standing membrane. The diffusion-migration rate of tetramethylammonium chloride

was very similar to sodium chloride when present in the same concentration, which indicated no influence of the size of the electrolyte conductor due to the high porosity.

Keywords: polypyrrole; graphene oxide; hybrid material; membrane; scanning electrochemical microscopy; electrochemical impedance spectroscopy.

---

* Corresponding author. Fax: +34 966528438; telephone: +34 966528412.

E-mail addresses: jamopue@doctor.upv.es (J. Molina), joboca@txp.upv.es (J. Bonastre), jaferse1@posgrado.upv.es (J. Fernández), delgaran@doctor.upv.es (A.I. del Río), fjcases@txp.upv.es (F. Cases).

1. Introduction

The discovery of conducting polymers in the 1970s led to a revolution in the field of materials science and different applications such as supercapacitors, LEDs, solar cells, field effect transistors, biosensors, etc., have been reported for the family of conducting polymers [1]. The isolation of graphene by K.S. Novoselov and A.K. Geim [2] has led to the last revolution in materials science due to its outstanding electronic, mechanical, optical and thermal properties [3]. Different applications in electronics, photonics, composite materials, energy storage, sensors or bio-applications have been studied [3]. The family of graphene materials is comprised of a range of different materials (graphene, graphene oxide, reduced graphene oxide, nitrogen doped graphene, etc.). Among the production methods of graphene derivatives, chemical methods for the production of graphene oxide (GO) have received particular attention due to its ease of operation and high capacity production [4]. This processing technique has the drawback

that GO is an insulating material due to the disrupted sp^2 structure. However, its posterior reduction leads to the partial restoration of the conducting sp^2 structure of graphene [5].

During the polymerization of pyrrole (Py) to form polypyrrole (PPy) (either chemically or electrochemically), positive charges are created in its structure (polarons and bipolarons). These charges need to be neutralized to maintain the electroneutrality principle; the charge compensation is produced by a counter ion (anion). Traditionally, organic counter ions (such as anthraquinone sulfonic acid) have been employed for such purpose [6], although the employment of inorganic counter ions has also been reported [6,7]. GO presents negative charges in its structure due to the presence of functional groups (carboxylic acids, hydroxyl groups, etc.) [8], reason why GO presents negative Zeta potential [9]. Its negative nature allows the incorporation of GO in the PPy matrix during polymerization, and the large size of GO sheets (typically in the order between hundreds of nm and several μm) prevents its expulsion from the PPy structure. This would be an advantage when compared with the employment of traditional organic counter ions (such as anthraquinone sulfonic acid with a size in the order of several Å), which suffer migration and are partially expulsed from the PPy structure, especially after deprotonation of PPy in basic media [10]. The combination of PPy with GO has been shown of interest for the production of composites with interesting properties for the development of supercapacitors [11,12], microbial fuel cells [13], counter electrode for dye-sensitized solar cells [14], Cr (VI) removal [15], etc. Chemical [15] and electrochemical methods of synthesis [11-14] of PPy/GO composites have been reported previously in bibliography.

Several studies have studied the transport properties across PPy films doped with organic [16-19] or inorganic counter ions [7]. However, up-to-date no study of this type

has been performed on PPy/GO films. The main objective of this work is to characterize the PPy/GO nanocomposite as a membrane material for the first time, to study the transport properties across it. Electrical characterization has been performed by electrochemical impedance spectroscopy (EIS) with the symmetric metal-PPy/GO-metal configuration. The electrochemical characterization of the free-standing PPy/GO films has been performed in solution by EIS and cyclic voltammetry (CV). Scanning electrochemical microscopy (SECM) has also been applied for the first time to study the electroactivity of PPy/GO hybrid materials obtained electrochemically.

2. Experimental

2.1. Reagents and materials

All reagents used were of analytical grade.

For the synthesis: Monolayer graphene oxide (GO) powder was acquired from Nanoinnova Technologies S.L. (Spain). The thickness of the GO flakes was in the order of 0.7-1.2 nm which demonstrates its monolayer nature, typical values for monolayer GO are around 1 nm [4]. Other characteristics of the GO employed in this work can be consulted on the web of the provider [20]. Analytical grade pyrrole (Py) was purchased from Merck.

For the characterization: Sulphuric acid (H_2SO_4) and potassium chloride (KCl) were purchased from Merck. Sodium chloride (NaCl) was supplied by Fluka. Hexaammineruthenium (III) chloride ($Ru(NH_3)_6Cl_3$), potassium ferrocyanide (III) $K_3Fe(CN)_6$ were used as received from Acrōs Organics. Tetramethylammonium chloride was purchased from Panreac.

When needed, solutions were deoxygenated by bubbling nitrogen (N_2 premier X50S). Ultrapure water was obtained from an Elix 3 Millipore-Milli-Q Advantage A10 system with a resistivity near to 18.2 MΩ·cm.

2.2. Synthesis of PPy/GO films

All electrochemical experiments were performed at room temperature with an Eco-Chemie Autolab PGSTAT302 potentiostat/galvanostat. Electrochemical synthesis of PPy/GO was performed in 2 $g \cdot L^{-1}$ GO/ 0.2 M Py aqueous solution. Firstly, the synthesis was performed on stainless steel (SS) electrodes employing a three-electrode configuration. When needed, the PPy/GO film was detached for the SS surface with the help of a sharp blade to obtain the membranes. The characteristics of SS electrode plates employed were: (plates of 2 cm × 3 cm × 0.1 cm); the chemical composition in weight (%) was: C ≤0.050, Si 0.750, Mn≤2.000, P 0.040, S 0.015, Cr 18–19, Cu 8.5–9, the rest of the composition corresponds to Fe. Before the electrosynthesis, SS electrodes were degreased with acetone, mechanically polished to obtain a smooth surface and then, cleaned with ultrapure water in an ultrasonic bath. The counter electrode was a SS mesh with cylindrical geometry to equalize the electric field around the working electrode. Electrochemical potential was referred to the Ag/AgCl (3.5 M KCl) reference electrode. Firstly, cyclic voltammetry (CV) technique was employed to determine the synthesis potential (0.86 V was the potential selected). Thereafter, potentiostatic synthesis was performed at 0.86 V until an electrical charge of 1 $C \cdot cm^{-2}$ was achieved.

2.3. Fourier transform infrared spectroscopy with attenuated total reflection (FTIR-ATR)

FTIR-ATR with horizontal mono-rebound attenuated total reflection accessory was performed with a Nicolet 6700 Spectrometer equipped with deuterated triglycine sulfate detector. An accessory with pressure control was used to equalize the pressure in the different solid samples. A prism of ZnSe was used and spectra were collected with a resolution of 4 cm^{-1}, 64 scans were averaged for each sample. GO powders were characterized to assign their different contributions.

2.4. Field emission scanning electron microscopy (FESEM) and energy dispersive X-ray analysis (EDX)

A Zeiss Ultra 55 FESEM was used to observe the morphology of the samples using an acceleration voltage of 3 kV. Energy dispersive X-ray (EDX) measurements were performed between 0 and 10 kV. An optical microscope Zeiss Discovery V.8 was employed to observe the mounting of the membrane on an adhesive tape.

2.5. Electrochemical impedance spectroscopy measurements

A two-electrode configuration was employed to measure the electronic conductivity of the PPy/GO films. The PPy/GO sample was located between two metals; one was the SS electrode where the film was grown and the other was Hg, applied as drops on the surface of the PPy/GO film. Hg is liquid and adapts to the surface topography of the electrode, thus allowing a better interfacial contact with the electrode material than when employing rigid metallic electrodes.

A standard three-electrode design was used to measure the EIS response of SS-PPy/GO electrodes in 0.1 M H_2SO_4 solutions. An asymmetrical configuration metal-sample-electrolyte was used. An Ag/AgCl (3.5 M KCl) electrode and Pt wire were used as reference electrode and counter electrode, respectively.

A four-electrode configuration was employed to measure the transport properties across the PPy/GO free-standing membrane. A two-compartment symmetrical electrochemical cell was employed to carry out the measurements. The membrane separated the two compartments. Two Pt electrodes were employed as auxiliary electrodes and two Ag/AgCl (3.5 M KCl) reference electrodes were employed to measure the potential. The measurements were performed in 0.50 M, 0.10 M, 0.05 M and 0.01 M NaCl solutions. 0.1 M tetramethylammonium solutions were used to test the effect of size of the ion on the diffusion-migration through the membrane.

EIS measurements were performed in the 10^5 to 10^{-2} Hz frequency range by using an Autolab PGSTAT302 potentiostat/galvanostat. The amplitude of the sinusoidal voltage was ± 10 mV. Each measurement was carried out at a constant imposed potential equal to the stabilized open circuit potential at the beginning of the experiment. The experimental results were also fitted using a non-linear least squares fitting minimization method by ZView software (version 2.7).

2.6. Scanning electrochemical microscopy (SECM)

SECM measurements were carried out with a scanning electrochemical microscope of Sensolytics. A three-electrode configuration cell consisting of a 25-µm-diameter Pt microelectrode, a Pt wire auxiliary electrode and an Ag/AgCl (3.5 M KCl) reference electrode. Measurements were performed in 0.01 M $Fe(CN)_6^{3-}$ / 0.1 M KCl and 0.01 M $Ru(NH_3)_6^{3+}$ / 0.1 M KCl solutions. All the experiments were carried out in an inert nitrogen atmosphere after deoxygenation by N_2 bubbling. The samples were glued to microscope slides with epoxy resin. The microelectrode operated at a potential of -0.4 V for $Ru(NH_3)_6^{3+}$, or 0 V for $Fe(CN)_6^{3-}$, at which the oxidized form of the redox mediator (Ox) is reduced (Red) at a diffusion controlled rate. Approach curves were obtained by

recording the tip reduction current as the Pt microelectrode tip was moved in z direction. Approach curves give us an indication of the electroactivity of the surface. These curves were compared to the theoretical positive feedback model. The substrate surface in all the measurements was at its open circuit potential (OCP). 2-D and 3-D representations of the array scans were obtained by positioning the microelectrode inside the influence of the electrochemical field, at a proper height over the substrate surface.

3. Results and discussion

3.1. Electrochemical synthesis

The electrochemical synthesis of PPy/GO on SS electrodes was performed in 0.2 M pyrrole and 2 $g \cdot L^{-1}$ GO aqueous solution. No additional electrolyte was added to the solution to avoid the incorporation of anions arising from the supporting electrolyte as counter ion in the PPy matrix; this approach has been also employed by other authors [11,12,21]. It should be taken into account that GO presents carboxylic acids in its structure, which can release H^+ that act as electrolyte to conduct the charges [22]. Fig. 1-a shows the characterization of the SS electrode in the synthesis solution. As can be seen, the current density increases with the number of scan. It is important to avoid over-oxidation of the polymer, for this reason the potential selected to carry out the synthesis was 0.86 V. This potential was sufficient to allow the formation of the PPy film as it was stated from SEM and FTIR results. Fig. 1-b shows the current density transient curve for the potentiostatic synthesis at 0.86 V of PPy/GO on SS electrode. Occasional N_2 bubbling was applied since precipitation of GO occurred with time, probably due to the adsorption of Py on the surface of GO due interactions such as π-π

interactions, electrostatic interactions, etc. For this reason graphene materials are employed as adsorbents of organic compounds [23]. The synthesis time (approximately 2 h) was so long due to the low conductivity of the media, hence requiring a longer deposition time. The currents obtained in CV or potentiostatic synthesis for the electrochemical synthesis of PPy/GO without additional electrolyte are lower than for the synthesis of PPy employing additional electrolyte [11]. Thus, a longer time of synthesis is required for the synthesis of PPy/GO without adding supporting electrolyte. However, this approach avoids the incorporation of electrolyte anions as counter ions in the structure of PPy as mentioned previously.

3.2. FTIR-ATR characterization

Fig. 2 shows the FTIR-ATR characterization of PPy/GO films. The spectrum of GO powders is also presented as reference. The main peaks observed for GO were: the band at 1720 cm^{-1} which was associated with the stretching vibrations of C=O bonds [24]. The peak at 1613 cm^{-1} was ascribed to C=C skeleton vibration from unoxidized sp^2 bonds [24]. The band at 1220 cm^{-1} was attributed to C-OH stretching vibrations, and finally the band around 1050 cm^{-1} was assigned to C-O stretching vibrations [24].

Afterwards, both sides of the PPy/GO films (the side in contact with the SS electrode and the one in contact with the solution) were characterized to see whether there were differences between them. Different bands attributed to PPy were observed, the most significant were [25]:

- The band around 1540 cm^{-1} which was associated to the pyrrole ring stretching vibration (C=C).
- C-C stretching vibration can be observed at 1450 cm^{-1}.

- The characteristic bands of the bending vibration of pyrrole can be observed at 775, 1037 and 1162 cm^{-1}.
- The band at 1092 cm^{-1} was attributed to the N^{+}-H in plane deformation.
- The band at 956 cm^{-1} was attributed to C-C out of plane deformation.

Regarding GO presence in the PPy/GO films, a band at 1700 cm^{-1} attributed to C=O stretching vibrations appeared in the spectra. This band suffered a displacement when compared with GO powders and it was due to the interaction of GO and PPy (π-π interactions and hydrogen bonding) [11], which confirmed the synthesis of the hybrid material.

Little difference was observed between the two sides of the PPy/GO sheets (the one in contact with the solution and the one in contact with the SS electrode). Only the intensity of the band at 1700 cm^{-1} varied. This could be due to the more planar structure of the side grown on the SS electrode side which would allow a better contact of the film with the ZnSe crystal employed to carry out the measurements. The measurements were performed in triplicate in different parts of the sample and the same tendency was observed for all of them.

3.3. FESEM and EDX

FESEM was employed to observe the morphology of the PPy/GO films. Fig. 3-a shows the micrograph of the side in contact with the SS electrode. It can be seen that the surface is very smooth with no mentionable features (when compared with the other side of the film). Fig. 3-b shows the inner structure of the coating, as can be seen the structure is very porous due to the incorporation of GO sheets during the polymerization of Py to produce PPy. Since no additional electrolyte was employed, the negative charges of GO compensate the positive charges created in the structure of PPy (polarons

and bipolarons). Fig. 3-c shows a magnified micrograph that shows the GO sheets coated with PPy. In Fig. 3-d, a micrograph showing ordered deposition of PPy/GO sheets in a punctual spot is presented, the self-assembly of different PPy/GO sheets was observed. The thickness of the PPy/GO sheets is below 20 nm. However, in general, the deposition was disordered as can be seen in Fig. 3-b and Fig. 3-c.

Fig. 4-a shows the FESEM characterization of the side of the PPy/GO film in contact with the synthesis solution. It can be seen that the morphology is totally different from the side in contact with the SS electrode. This side is rougher and the presence of GO sheets can be easily observed. In the case of the side in contact with the SS electrode it seems that the first step is the PPy polymerization which produced a fine structure. Later, GO sheets were progressively incorporated in the structure of the film as it grows. Fig. 4-b shows a magnified micrograph where the PPy structure can be observed. In Fig. 4-c, a GO sheet can be observed in the center of the image. It can be seen that PPy globules are progressively growing on its surface. Fig. 4-d shows the presence of different GO sheets on the PPy structure. The wrinkles of GO help to locate them [26] on the surface of the PPy/GO coating.

Fig. 5 and Fig. 6 shows the EDX characterization of the PPy/GO film. The elements detected were C, O, N, S and Cl. S and Cl are impurities that arise from the synthesis process of GO that employs sulfuric acid among other strong acids and oxidants. The presence of N indicates the formation of the PPy coating. The presence of O is mainly attributed to GO, although it could also be present in PPy structure due to oxidation of chain structure. Fig. 5 also shows the element map distribution of the major elements. There was a uniform distribution of all the elements on the side in contact with the SS electrode. On the other hand, the side in contact with the solution (Fig. 6) showed the accumulation of C and O in the zones where GO sheets where deposited. Taking into

account the FESEM and EDX data, this would indicate that in the mechanism of film formation, PPy film is firstly formed on the SS electrode and thereafter, GO sheets are progressively incorporated within the growing film. As can be seen in both EDX spectra (Fig. 5-e and Fig. 6-e), significant differences in the composition of both sides of the film were not observed. X-ray are able to penetrate several microns inside the sample and hence a bulk composition is obtained instead of a surface one.

3.4. EIS characterization

EIS technique with the two-electrode configuration was employed to measure the electronic conductivity of the PPy/GO film. The metal-PPy/GO-metal symmetrical configuration was employed for this purpose. Fig. 7 shows the corresponding Nyquist plot obtained. The electrical behavior of the material (black dots) can be modeled as a RC (resistance-capacitor) system. The characteristic frequency for this time constant was 16000 Hz. The electronic resistance for the PPy-GO film was Rf = 107 $\Omega \cdot cm^2$. Considering the thickness of the film, noting Fig. 3-b (~5 μm), the electronic conductivity was $4.7 \cdot 10^{-6}$ S/cm, higher than the value obtained for PPy/$PW_{12}O_{40}^{3-}$ membrane (~$7.5 \cdot 10^{-8}$ S/cm) [7]. The capacitance of the PPy-GO film as dielectric material (without solution) was Cf = $6.3 \cdot 10^{-8}$ F/cm^2.

The four-electrode symmetrical configuration was employed to measure the ion conducting properties through PPy/GO free-standing membrane. First, PPy/GO film was detached from the SS electrode and was mounted between an adhesive tape that had a hole to communicate both sides of the electrochemical cell. Fig. 8-a shows an optical microscope image of the side of the membrane that was grown on the stainless steel electrode. Fig. 8-b shows the side of the membrane that was in contact with the synthesis solution. Since the side in contact with the SS electrode was smoother it

reflects more light than the other side of the membrane, which was rougher and reflects less light. The size of the exposed membrane area was 1.44 mm^2. The electrolyte used was 0.1 M H_2SO_4. Fig. 7 (red dots) shows the Nyquist plot for the symmetrical configuration 0.1 M H_2SO_4/PPy-GO/0.1 M H_2SO_4, i.e. the membrane ionic impedance. The high frequency loop is due to polymer/electrolyte interface. The low frequency loop is due to diffusion-migration of ionic-electronic charge carriers (counter-ions and polarons) [27]. The overall ionic resistance of the membrane has a value of 4 $\Omega \cdot cm^2$.

Once the separate electrical and ionic behavior had been analyzed by the two symmetrical configurations, metal-PPy/GO-metal and solution-PPy/GO-solution, the next step was the analysis of the overall electrical response with a conventional three-electrode cell. Figs. 9-a, and 9-b show the Nyquist and Bode plots for the PPy-GO/SS electrode immersed in 0.1 M H_2SO_4 solution. The high frequency loop (Fig. 9-a) has a characteristic frequency similar (resistance and capacitance also similar) to the electrical response obtained in Fig. 7. Therefore, this time constant is also due to the electronic properties of the PPy/GO film in the asymmetric configuration metal-PPy/GO-solution. The different values were fitted using a non-linear least squares fitting minimization method by ZView software. The electronic resistance for the film was 100 $\Omega \cdot cm^2$ and the corresponding capacity was $9.1 \cdot 10^{-8}$ F/cm^{-2}.

Other relaxation process appears at middle-low frequencies (1-0.01 Hz). Seeing the Bode diagram in Fig. 9-b, a phase angle of about -45º was obtained at 0.01 Hz. This shows in principle Warburg behavior. Taking into account that there are not redox couples in solution, the following equivalent electrical circuit is proposed in the inset of Fig. 9-b. This equivalent circuit is composed of:

- Rs: Electrolyte resistance.

- Rf: Electronic resistance of the PPy/GO film.

- Cf: Capacitance of the PPy/GO film.

- Wd: Warburg impedance due to counter-ion + polaron diffusion-migration. W-R: diffusion-migration resistance. W-T: l^2/D (s), l: length of the diffusion-migration layer, D: binary counter-ion + polaron diffusion-migration coefficient. W-P: Warburg exponent.

The second loop at low frequencies is due to diffusion-migration process. Migration-diffusion resistance is about 11 $\Omega \cdot cm^2$ (4 $\Omega \cdot cm^2$ for ionic symmetric configuration in Fig.7, and 13 $\Omega \cdot cm^2$ for dc resistance of the membrane in section 3.5). Therefore, the rate-determining step is the low electronic conductivity of the PPy/GO film (100 $\Omega \cdot cm^2$).

3.4.1. EIS response of PPy/GO free-standing films in NaCl solutions of different concentration and $(CH_3)_4N^+Cl^-$

The PPy/GO free-standing film was placed in a symmetrical configuration between two ionic solutions and an ac voltage was applied. The electrical response is due to the following phenomena [19]:

- Re: Electrolyte resistance

- Zi: Ion transfer impedance at the polymer/electrolyte interface.

- Zp: Ion transport impedance within the film.

The physical phenomena of PPy free-standing films may be modeled according to the equivalent circuit [19] showed in Fig. 10.

To study the electric properties of the PPy/GO membranes in relation to electrolyte concentration, four different NaCl solutions were prepared with the following concentrations: 0.01, 0.05, 0.10 and 0.50 M. To see the effect of the size of the ion on the ion diffusion, a 0.10 M tetramethylammonium chloride solution was also prepared

and tested. Fig. 11 shows the Nyquist plot for a PPy-GO membrane immersed in 0.1 M NaCl solution with the symmetrical configuration. Two loops appeared in the diagram due to two relaxation processes. The high-middle frequencies loop is related to the ionic exchange between PPy/GO membrane and the solution. The diagram shows a second loop at low frequencies. This time constant is due to the counter-ion diffusion in the bulk polymeric film. This diffusion presented transmissive boundary conditions, since a resistive behavior at very low frequencies is shown in the Nyquist plot, typical in this ion non-blocking interface.

Fig. 12 shows the Bode plots for PPy/GO membrane that was immersed in NaCl and tetramethylammonium chloride solutions with different concentrations: 0.01, 0.05, 0.10 and 0.50 M. Nyquist plots are not shown because the shape was very similar to Fig. 11. Two time constants can be appreciated in the plot phase vs. frequency for all the assays. The high-middle frequency range (10,000–1 Hz) corresponds to the ionic exchange impedance between membrane and solution, as it was commented before. This time constant changed to lower frequencies when the NaCl solution was more diluted. The middle-low frequency range (1–0.01 Hz) is due to diffusion-migration of counter-ions in the polymeric membrane. The time constant changed to lower frequencies when the NaCl solution was more diluted. Seeing the impedance modulus vs. frequency plot, the impedance modulus increased when the membrane was immersed in more diluted solutions for all the frequencies analyzed. Therefore, the two relaxation processes (ionic exchange impedance and diffusion-migration of counter-ions within the membrane) were slower when the NaCl concentration was lower.

To analyze the effect of the electrolyte ions size, the PPy-GO membrane was immersed in 0.10 M $(CH_3)_4N^+Cl^-$ solution. Bode plots in Fig. 12 show how both, ionic exchange and diffusion-migration presented a similar behavior for 0.1 M $(CH_3)_4N^+Cl^-$ solution in

comparison to 0.1 M NaCl one. The trimethylammonium ion size is much larger than chloride and sodium ions. This fact confirms the high porosity of the PPy/GO films as it was discussed in section 3.3 (Fig. 3-b).

3.5. Cyclic voltammetry characterization

Cyclic voltammetry was also performed in 0.5 M H_2SO_4 solution with and without the membrane using the 4-electrode configuration (Fig. 13). The voltammograms showed a linear resistive response. The slope of the voltammogram without the membrane was related to the resistance of the electrolyte and the electrode configuration employed; the calculated resistance was 60 Ω. When the PPy/GO membrane was located, there was a decrease of the current intensity measured, indicating an increase of the resistance due to the presence of the membrane. The calculated dc resistance of the membrane after subtracting the electrochemical configuration was 13 Ω. Taking into account the thickness of the membrane (5 μm) and the membrane area (1.44 mm^2), the ionic dc (direct current) conductivity of the PPy-GO membrane was: $1.6 \cdot 10^{-3}$ S/cm. This value is two orders of magnitude higher than in previous work for PPy/$PW_{12}O_{40}^{3-}$ membrane ($1.7 \cdot 10^{-5}$ $S \cdot cm^{-1}$) [7].

Taking into account the high porosity obtained that enhances the ion conductivity through the membrane, the high surface area and the conductivity of the composite material there are several applications where these materials can be used. One of them is the electroanalysis of heavy metals, where the high surface area and functional groups of GO and PPy help in the processes of pre-concentration and stripping of metal ions [28-30]. The 3-D architecture obtained helps in enhancing the surface area which is beneficial for different purposes such as adsorption, detection, etc. [31]. The incorporation of metal nanoparticles inside this 3-D structure has not been reported and

would be advantageous for the electroanalysis of heavy metals. The high porosity of the PPy/GO hybrid material shows that the size of the counter ion has no effect on the ionic diffusion-migration, which would allow the easy adsorption of metal precursors ($AuCl^{4-}$, $PtCl_6^{2-}$, Ag^{+}, etc.) inside the 3-D structure. Thereafter, these precursors would be reduced to metal nanoparticles chemically or electrochemically (given that the composite material is electrically conducting). Other possible approach is to perform the synthesis of the nanoparticles and PPy/GO simultaneously. The synergies provided by PPy, GO and metal nanoparticles would produce sensors with decreased limit of detection. Other applications, if Pt nanoparticles were to be synthesized, include electrode material for fuel cells (methanol or ethanol oxidation) [32], etc. More work is in progress to evaluate the application of these materials. The mechanical stability of the PPy/GO hybrid material as a free-standing membrane is limited due to its highly porous structure and low thickness of the film, although when supported on an electrode material is good. In order to increase the mechanical stability of the free-standing film, one approach that can be employed is the use of higher synthesis charges to obtain thicker films. Values of up to 5 $C \cdot cm^{-2}$ have been reported in bibliography with the outcome of good mechanical properties [11]. For the different applications mentioned previously, the hybrid material will be used as a deposited film on a supporting electrode, which allows the electron transfer. Different supporting materials are being studied at present for this purpose.

3.6. SECM characterization

SECM was employed to test the electroactivity of the PPy/GO films. The characterization by SECM of PPy/GO films obtained electrochemically has not been reported in bibliography and only our previous work dealt with the SECM

characterization of PPy/GO obtained chemically [25]. Few works have applied this technique to study graphene materials [22,24,26,33-37]. SECM is a powerful technique that can be employed to measure the electroactivity [22,24,26,34,36], electron transfer kinetics [33,35] or even conductivity [37] of graphene materials. The technique was operated in the feedback mode which is based on measuring the current on the surface of a microelectrode as the microelectrode approaches the surface of the substrate subject of study [34]. Fig. 14-a shows the approach curves obtained employing PPy/GO film supported on SS electrode as substrate. Two different redox mediators were employed ($Fe(CN)_6^{3-}$ and $Ru(NH_3)_6^{3+}$). For both redox mediators, positive feedback was obtained. The behavior was very close to the ideal positive feedback of a conducting material.

The positive feedback model curve was obtained according to equation 1. According to Rajendran el al. [38], Pade's approximation gives a close and simple equation with less relative error for all distances and is valid for RG > 10. The approximate formula of the steady-state normalized current assuming positive feedback for finite conductive substrate together with finite insulating glass thickness is:

$$I_T{}^C = \left[\frac{1 + 1.5647/L + 1.316855/L^2 + 0.4919707/L^3}{1 + 1.1234/L + 0.626395/L^2} \right] \quad (1)$$

The membrane was detached from the SS electrode and was also analyzed to discard any contribution for the metallic substrate. In this case, only the $Fe(CN)_6^{3-}$ redox mediator was employed to carry out the measurements since similar response was obtained for both redox mediators. As can be seen in Fig. 14-b the PPy/GO membrane shows also positive feedback close to the ideal conducting behavior. Both sides of the membrane were analyzed (the one in contact with the SS electrode and the one in contact with the solution). Similar behavior was obtained for both sides of the PPy/GO membrane analyzed, indicating a similar electroactivity degree for both sides. The

degree of positive feedback and the adjust to the theoretical model for positive feedback was superior for PPy/GO electrochemically obtained than when PPy/GO composites were obtained chemically [25]. This indicates a higher electroactivity of PPy/GO synthesized electrochemically.

Fig. 15 shows the 2-D and 3-D representations of PPy/GO supported on SS electrode. As can be seen, the values of normalized current are between 1.26 and 1.58 (within the positive feedback zone). This indicates a homogeneous distribution of the conducting material. The variations in the value of positive feedback can be attributed to the variations in morphology and topography observed in the side in contact with the solution, as observed in micrographs of Fig. 4.

4. Conclusions

PPy/GO coatings were obtained on stainless steel electrodes by potentiostatic synthesis. FTIR-ATR showed the formation of the hybrid material and the effective incorporation of GO in the structure. As observed by FESEM, the structure of the coating was very porous due to the incorporation of GO that was intercalated in the PPy structure. Differences in morphology between the side grown on the stainless steel electrode and the side in contact with the solution were observed. It seems that the first stage is the formation of a PPy film and progressively GO sheets are incorporated within the coating.

Conductivity of the films was studied by EIS with the symmetric metal-PPy/GO-metal configuration and the electronic conductivity obtained was $4.7 \cdot 10^{-6}$ S/cm. The measurement with the asymmetrical metal-PPy/GO-solution configuration showed the appearance of two time constants attributed to the electron transport and the diffusion-

migration processes. The rate-determining step was the electronic transport in the PPy/GO film. The transport study across PPy/GO free standing film acting as a membrane was analyzed by means of EIS in solution with the solution-PPy/GO-solution configuration. The ionic dc conductivity of the PPy/GO membrane was $1.6 \cdot 10^{-3}$ S/cm. PPy/GO membranes are excellent ionic conductors due to its high porosity. No difference was observed when employing different size ions for the study of ion diffusion, which indicates that the pore size is high enough to allow differences to be observed. Due to the good diffusion-migration properties of the material, its conductivity and high surface area, it can be used for electrochemical applications such as sensors or as a support to deposit other catalytic materials for electrochemical applications.

SECM technique showed that the material was electroactive and behaved like an ideal conductor showing positive feedback. The 2-D and 3-D mapping of surface electroactivity showed a homogeneous distribution of the material.

Role of the funding source

The funding sources had no involvement in the study design; in the collection, analysis and interpretation of data; in the writing of the report; and in the decision to submit the article for publication.

Acknowledgements

Authors wish to thank to the Spanish Ministerio de Ciencia e Innovación (contract CTM2011-23583) for the financial support. J. Molina is grateful to the Conselleria

d'Educació, Formació i Ocupació (Generalitat Valenciana) for the Programa VALi+D Postdoctoral Fellowship (APOSTD/2013/056). A.I. del Río is grateful to the Spanish Ministerio de Ciencia y Tecnología for her FPI fellowship. Electron Microscopy Service of the UPV (Universitat Politècnica de València) is gratefully acknowledged for help with FESEM and EDX characterization.

References

[1] M. Ates, T. Karazehira, A.S. Sarac, Conducting polymers and their applications, Curr. Phys. Chem. 2 (2012) 224-240.

[2] K.S. Novoselov, A.K. Geim, S.V. Morozov, D. Jiang, Y. Zhang, S.V. Dubonos, I.V. Grigorieva, A.A. Firsov, Electric field effect in atomically thin carbon films, Science 306 (2004) 666-669.

[3] K.S. Novoselov, V.I. Fal'ko, L. Colombo, P.R. Gellert, M.G. Schwab, K.Kim, A roadmap for graphene, Nature 490 (2012) 192-200.

[4] S. Park, R.S. Ruoff, Chemical methods for the production of graphenes, Nat. Nanotechnol. 4 (2009) 217-224.

[5] S. Pei, H.-M. Cheng, The reduction of graphene oxide, Carbon 50 (2012) 3210-3228.

[6] J. Molina, A.I. del Río, J. Bonastre, F. Cases, Chemical and electrochemical polymerisation of pyrrole on polyester textiles in presence of phosphotungstic acid, Eur. Polym. J. 44 (2008) 2087-2098.

[7] J. Bonastre, J. Molina, J.C. Galván, F. Cases, Characterization of polypyrrole/phosphotungstate membranes by electrochemical impedance spectroscopy, Synth. Met. 187 (2014) 37-45.

[8] D.R. Dreyer, S. Park, C.W. Bielawski, R.S. Ruof, The chemistry of graphene oxide, Chem. Soc. Rev. 39 (2010) 228-240.

[9] G.G. Wallace, R.B. Kaner, M. Muller, S. Gilje, D. Li, Processable aqueous dispersions of graphene nanosheets, Nat. Nanotechnol. 4 (2009) 25-29.

[10] J. Molina, J. Fernández, A.I. del Río, R. Lapuente, J. Bonastre, F. Cases, Stability of conducting polyester/polypyrrole fabrics in different pH solutions. Chemical and electrochemical characterization, Polym. Degrad. Stab. 95 (2010) 2574-2583.

[11] C.Z. Zhu, J.F. Zhai, D. Wen, S.J. Dong, Graphene oxide/polypyrrole nanocomposites: one-step electrochemical doping, coating and synergistic effect for energy storage, J. Mater. Chem. 22 (2012) 6300-6306.

[12] H.-H. Chang, C.-K. Chang, Y.-C. Tsai, C.-S. Liao, Electrochemically synthesized graphene/polypyrrole composites and their use in supercapacitor, Carbon 2 (2012) 2331-2336.

[13] Z. Lv, Y. Chen, H. Wei, F. Li, Y. Hu, C. Wei, C. Feng, One-step electrosynthesis of polypyrrole/graphene oxide composites for microbial fuel cell application, Electrochim. Acta 111 (2013) 366-373.

[14] S.P. Lim, A. Pandikumar, Y.S. Lim, N.M. Huang, H.N. Lim, In-situ electrochemically deposited polypyrrole nanoparticles incorporated reduced graphene oxide as an efficient counter electrode for platinum-free dye-sensitized solar cells, Sci. Rep. 4 (2014) 5305.

[15] S. Li, X. Lu, Y. Xue, J. Lei, T. Zheng, C. Wang, Fabrication of polypyrrole/graphene oxide composite nanosheets and their applications for Cr(VI) removal in aqueous solution, J. Mater. Chem. 22 (2012) 6300-6306.

[16] C. Ehrenbeck, K. Jüttner, S. Ludwig, G. Paasch, The electrochemical impedance of a free-standing polypyrrole membrane, Electrochim. Acta 43 (1998) 2781-2789.

[17] C. Ehrenbeck, K. Jüttner, Ion conductivity and permselectivity measurements of polypyrrole membranes at variable states of oxidation, Electrochim. Acta 41 (1996) 1815-1823.

[18] C. Deslouis, T. El Moustafid, M.M. Musiani, B. Tribollet, Mixed ionic-electronic conduction of a conducting polymer film. AC impedance study of polypyrrole, Electrochim. Acta 41 (1996) 1343-1349.

[19] C. Deslouis, M.M. Musiani, B. Tribollet, Free-standing membranes for the study of electrochemical reactions occurring at conducting polymer/electrolyte interfaces, J. Phys. Chem. 100 (1996) 8994-8999.

[20] http://www.nanoinnova.com/Product/Details/24. Last accessed 08.04.2016.

[21] W. Liu, Y. Fang, P. Xu, Y. Lin, X. Yin, G. Tang, M. He, Two-step electrochemical synthesis of polypyrrole/reduced graphene oxide composites as efficient Pt-free counter electrode for plastic dye-sensitized solar cells, ACS Appl. Mater. Interfaces 6 (2014) 16249-16256.

[22] J. Molina, J. Fernández, A.I. del Río, J. Bonastre, F. Cases, Synthesis of Pt nanoparticles on electrochemically reduced graphene oxide by potentiostatic and alternate current methods, Mater. Charact. 89 (2014) 56-68.

[23] F. Perreault, A.F. de Faria, M. Elimelech, Environmental applications of graphene-based nanomaterials, Chem. Soc. Rev. 44 (2015) 5861-5896.

[24] J. Molina, J. Fernandez, J.C. Ines, A.I. del Rio, J. Bonastre, F. Cases, Electrochemical characterization of reduced graphene oxide-coated polyester fabrics, Electrochim. Acta 93 (2013) 44-52.

[25] J. Molina, A. Zille, J. Fernández, A.P. Souto, J. Bonastre, F. Cases, Conducting fabrics of polyester coated with polypyrrole and doped with graphene oxide, Synth. Met. 204 (2015) 110-121.

[26] J. Molina, J. Fernández, A.I. del Río, J. Bonastre, F. Cases, Chemical and electrochemical study of fabrics coated with reduced graphene oxide, Appl. Surf. Sci. 279 (2013) 46-54.

[27] C. Deslouis, M.M. Musiani, B. Tribollet, M.A. Vorotyntsev, Comparison of the AC impedance of conducting polymer films studied as electrode-supported and freestanding membranes, J. Electrochem. Soc. 142 (1995) 1902-1908.

[28] Z.-Q. Zhao, X. Chen, Q. Yang, J.-H. Liu, X.-J. Huang, Selective adsorption toward toxic metal ions results in selective response: electrochemical studies on a polypyrrole/reduced graphene oxide nanocomposite, Chem. Commun. 48 (2012) 2180-2182.

[29] R. Seenivasan, W.-J. Chang, S. Gunasekaran, Highly sensitive detection and removal of lead ions in water using cysteine-functionalized graphene oxide/polypyrrole nanocomposite film electrode, ACS Appl. Mater. Interfaces 7 (2015) 15935-15943.

[30] Z.-Q. Zhao, X. Chen, Q. Yang, J.-H. Liu, X.-J. Huang, Beyond the selective adsorption of polypyrrole-reduced graphene oxide nanocomposite toward Hg^{2+}: Ultra-sensitive and -selective sensing Pb^{2+} by stripping voltammetry, Electrochem. Commun. 23 (2012) 21-24.

[31] Y. Shen, Q. Fang, B. Chen, Environmental applications of three-dimensional graphene-based macrostructures: Adsorption, transformation, and detection, Environ. Sci. Technol. 49 (2015) 67-84.

[32] W. Zhao, X. Zhou, Z. Xue, B. Wu, X. Liu, X. Lu, Electrodeposition of platinum nanoparticles on polypyrrole-functionalized graphene, J. Mater. Sci. 48 (2013) 2566-2573.

[33] J.-H. Zhong, J. Zhang, X. Jin, J.-Y. Liu, Q. Li, M.-H. Li, W. Cai, D.-Y. Wu, D. Zhan, B. Ren, Quantitative correlation between defect density and heterogeneous

electron transfer rate of single layer graphene, J. Am. Chem. Soc. 136 (2014) 16609-16617.

[34] J. Molina, J. Fernández, C. García, A.I. del Río, J. Bonastre, F. Cases. Electrochemical characterization of electrochemically reduced graphene coatings on platinum. Electrochemical study of dye adsorption, Electrochim. Acta 166 (2015) 54-63.

[35] C. Tan, J. Rodríguez-López, J.J. Parks, N.L. Ritzert, D.C. Ralph, H.D. Abruña, Reactivity of monolayer chemical vapor deposited graphene imperfections studied using scanning electrochemical microscopy, ACS Nano 6 (2012) 3070-3079.

[36] S. Rapino, E. Treossi, V. Palermo, M. Marcaccio, F. Paolucci, F. Zerbetto, Playing peekaboo with graphene oxide: a scanning electrochemical microscopy investigation, Chem. Commun. 50 (2014) 13117-13120.

[37] J. Azevedo, C. Bourdillon, V. Derycke, S. Campidelli, C. Lefrou, R. Cornut, Contactless surface conductivity mapping of graphene oxide thin films deposited on glass with scanning electrochemical microscopy, Anal. Chem. 85 (2013) 1812-1818.

[38] L. Rajendran, S.P. Ananthi, Analysis of positive feedback currents at the scanning electrochemical microscope, J. Electroanal. Chem. 561 (2004) 113-118.

Figure captions

Fig. 1. Electrochemical synthesis of PPy/GO on stainless steel electrodes in 2 $g \cdot L^{-1}$ GO and 0.2 M pyrrole solution. a) Cyclic voltammetry synthesis. b) Current density transient curve for potentiostatic synthesis. Start potential: 0 V, synthesis potential: 0.86 V, Q = 1 $C \cdot cm^{-2}$.

Fig. 2. FTIR-ATR spectra of GO powders and PPy/GO film electrochemically synthesized. The two sides of the PPy/GO film (the side in contact with the stainless steel electrode and the one in contact with the synthesis solution were analyzed). Measured with monorebound ZnSe prism, resolution 4 cm^{-1}, 64 scans.

Fig. 3. FESEM micrographs of PPy/GO film (side corresponding to the stainless steel interface) (a) (x 0.5 K), (b) (x 10 K), (c) (x 18.6 K), (d) (x 185 K).

Fig. 4. FESEM micrographs of PPy/GO film (side corresponding to the electrolyte interface) (a) (x 0.5 K), (b) (x 20 K), (c) (x 20 K), (d) (x 20 K).

Fig. 5. a) SEM micrograph, b) C, c) O and d) N distribution element maps, e) EDX spectra of PPy/GO film, side in contact with the stainless steel electrode. Acquisition time: 100 s.

Fig. 6. a) SEM micrograph, b) C, c) O and d) N distribution element maps, e) EDX spectra of PPy/GO film, side in contact with the stainless steel electrode. Acquisition time: 100 s.

Fig. 7. Nyquist plots for (•) symmetrical configuration metal/PPy-GO/metal and (⁻) fitting of experimental data, exposed electrode area, 1 cm^2, (•) symmetrical configuration 0.1 M H_2SO_4/PPy-GO/0.1 M H_2SO_4 (inset: magnified zone). Exposed electrode area, 1.44 mm^2. Frequency range from 10^5 to 10^{-2} Hz.

Fig. 8. Optical microscope image of the two sides of the PPy/GO membrane located between an adhesive tape. a) Side in contact with the stainless steel electrode, b) Side in contact with the synthesis solution.

Fig. 9. a) Nyquist and b) Bode plots for (•) asymmetrical configuration metal-PPy/GO-0.1 M H_2SO_4 and (–) fitting of experimental data. Frequency range from 10^5 to 10^{-2} Hz. Exposed electrode area, 1 cm^2.

Fig. 10. Electrical circuit for PPy/GO free-standing films in symmetrical configuration solution/membrane/solution.

Fig. 11. Nyquist plots for PPy/GO membrane in 0.1 M NaCl solution. Exposed membrane area: 1.44 mm^2. Frequency range from 10^4 to 10^{-2} Hz. (•) Experimental data. (–) Fitting data. Inset: Electrical circuit for PPy/GO free-standing films in symmetrical configuration solution/membrane/solution.

Fig. 12. Bode plots for PPy/GO membrane in 0.01, 0.05, 0.1 and 0.5 M NaCl, and 0.1 M $(CH_3)_4N^+Cl^-$ solutions. Exposed membrane area: 1.44 mm^2. Frequency range from 10^4 to 10^{-2} Hz.

Fig. 13. Cyclic voltammograms obtained in a 4-electrode arrangement in 0.5 M H_2SO_4 solution, scan rate 50 $mV \cdot s^{-1}$. Obtained without PPy/GO and with PPy/GO membrane. Exposed membrane area 1.44 mm^2.

Fig. 14. Approaching curves for a) PPy/GO deposited on stainless steel, b) PPy/GO membrane detached from the stainless steel electrode. The theoretical positive feedback model has been included as a continuous black line. The redox mediators employed were $Fe(CN)_6^{3-}$ in 0.1 M KCl, and $Ru(NH_3)_6^{3+}$ in 0.1 M KCl. Approaching curves obtained with a 25 µm diameter Pt tip. The tip potentials were 0 V and -0.4 V for $Fe(CN)_6^{3-}$ and $Ru(NH_3)_6^{3+}$, respectively. The approach rate was 20 $\mu m \cdot s^{-1}$. The area employed was 0.7 cm^2 for a) and 10 mm^2 for b).

Fig. 15. 2-D (a) and 3-D (b) constant height SECM images of PPy/GO on SS electrode. 0.7 cm^2 geometrical area sample, images were taken with a 25 µm diameter microelectrode, in 0.01 M $Fe(CN)_6^{3-}$ and 0.1 M KCl at a constant height of 20 µm. The tip potential was 0 V, the scan rate was 50 $\mu m \cdot s^{-1}$ in comb mode; lengths of x and y lines were 200 µm x 200 µm with increments of 10 µm.

Electrochemical synthesis of polypyrrole doped with graphene oxide and its electrochemical characterization as membrane material

J. Molina, J. Bonastre, J. Fernández, A.I. del Río, F. Cases*

Departamento de Ingeniería Textil y Papelera, EPS de Alcoy, Universitat Politècnica de València, Plaza Ferrándiz y Carbonell s/n, 03801 Alcoy, Spain

Abstract

Polypyrrole (PPy) doped with graphene oxide (GO) has been electrochemically obtained by potentiostatic synthesis and its electrochemical behavior as membrane material has been studied for the first time. Fourier transform infrared spectroscopy with attenuated total reflection showed the formation of the hybrid material due to presence of PPy and GO bands. Field emission scanning electron microscopy micrographs showed the effective incorporation of GO sheets and the formation of a 3-D porous material with high surface area. Scanning electrochemical microscopy of PPy/GO films showed positive feedback close to the ideal conducting behavior, indicating a good electroactivity. Electrochemical impedance spectroscopy (EIS) was employed to measure the electrochemical properties of the coatings by two-, three-, and four-electrode configurations. The electronic conductivity of PPy/GO film, measured between two metallic conductors, was $4.7 \cdot 10^{-6}$ S/cm. Its ionic conductivity was superior ($1.6 \cdot 10^{-3}$ S/cm) due to the high porosity of the material as demonstrated by cyclic voltammetry and EIS measurements, where the PPy/GO film was employed as a free-standing membrane. The diffusion-migration rate of tetramethylammonium chloride

was very similar to sodium chloride when present in the same concentration, which indicated no influence of the size of the electrolyte conductor due to the high porosity.

Keywords: polypyrrole; graphene oxide; hybrid material; membrane; scanning electrochemical microscopy; electrochemical impedance spectroscopy.

---

* Corresponding author. Fax: +34 966528438; telephone: +34 966528412.

E-mail addresses: jamopue@doctor.upv.es (J. Molina), joboca@txp.upv.es (J. Bonastre), jaferse1@posgrado.upv.es (J. Fernández), delgaran@doctor.upv.es (A.I. del Río), fjcases@txp.upv.es (F. Cases).

1. Introduction

The discovery of conducting polymers in the 1970s led to a revolution in the field of materials science and different applications such as supercapacitors, LEDs, solar cells, field effect transistors, biosensors, etc., have been reported for the family of conducting polymers [1]. The isolation of graphene by K.S. Novoselov and A.K. Geim [2] has led to the last revolution in materials science due to its outstanding electronic, mechanical, optical and thermal properties [3]. Different applications in electronics, photonics, composite materials, energy storage, sensors or bio-applications have been studied [3]. The family of graphene materials is comprised of a range of different materials (graphene, graphene oxide, reduced graphene oxide, nitrogen doped graphene, etc.). Among the production methods of graphene derivatives, chemical methods for the production of graphene oxide (GO) have received particular attention due to its ease of operation and high capacity production [4]. This processing technique has the drawback

that GO is an insulating material due to the disrupted sp^2 structure. However, its posterior reduction leads to the partial restoration of the conducting sp^2 structure of graphene [5].

During the polymerization of pyrrole (Py) to form polypyrrole (PPy) (either chemically or electrochemically), positive charges are created in its structure (polarons and bipolarons). These charges need to be neutralized to maintain the electroneutrality principle; the charge compensation is produced by a counter ion (anion). Traditionally, organic counter ions (such as anthraquinone sulfonic acid) have been employed for such purpose [6], although the employment of inorganic counter ions has also been reported [6,7]. GO presents negative charges in its structure due to the presence of functional groups (carboxylic acids, hydroxyl groups, etc.) [8], reason why GO presents negative Zeta potential [9]. Its negative nature allows the incorporation of GO in the PPy matrix during polymerization, and the large size of GO sheets (typically in the order between hundreds of nm and several μm) prevents its expulsion from the PPy structure. This would be an advantage when compared with the employment of traditional organic counter ions (such as anthraquinone sulfonic acid with a size in the order of several Å), which suffer migration and are partially expulsed from the PPy structure, especially after deprotonation of PPy in basic media [10]. The combination of PPy with GO has been shown of interest for the production of composites with interesting properties for the development of supercapacitors [11,12], microbial fuel cells [13], counter electrode for dye-sensitized solar cells [14], Cr (VI) removal [15], etc. Chemical [15] and electrochemical methods of synthesis [11-14] of PPy/GO composites have been reported previously in bibliography.

Several studies have studied the transport properties across PPy films doped with organic [16-19] or inorganic counter ions [7]. However, up-to-date no study of this type

has been performed on PPy/GO films. The main objective of this work is to characterize the PPy/GO nanocomposite as a membrane material for the first time, to study the transport properties across it. Electrical characterization has been performed by electrochemical impedance spectroscopy (EIS) with the symmetric metal-PPy/GO-metal configuration. The electrochemical characterization of the free-standing PPy/GO films has been performed in solution by EIS and cyclic voltammetry (CV). Scanning electrochemical microscopy (SECM) has also been applied for the first time to study the electroactivity of PPy/GO hybrid materials obtained electrochemically.

2. Experimental

2.1. Reagents and materials

All reagents used were of analytical grade.

For the synthesis: Monolayer graphene oxide (GO) powder was acquired from Nanoinnova Technologies S.L. (Spain). The thickness of the GO flakes was in the order of 0.7-1.2 nm which demonstrates its monolayer nature, typical values for monolayer GO are around 1 nm [4]. Other characteristics of the GO employed in this work can be consulted on the web of the provider [20]. Analytical grade pyrrole (Py) was purchased from Merck.

For the characterization: Sulphuric acid (H_2SO_4) and potassium chloride (KCl) were purchased from Merck. Sodium chloride (NaCl) was supplied by Fluka. Hexaammineruthenium (III) chloride ($Ru(NH_3)_6Cl_3$), potassium ferrocyanide (III) $K_3Fe(CN)_6$ were used as received from Acrōs Organics. Tetramethylammonium chloride was purchased from Panreac.

When needed, solutions were deoxygenated by bubbling nitrogen (N_2 premier X50S). Ultrapure water was obtained from an Elix 3 Millipore-Milli-Q Advantage A10 system with a resistivity near to 18.2 MΩ·cm.

2.2. Synthesis of PPy/GO films

All electrochemical experiments were performed at room temperature with an Eco-Chemie Autolab PGSTAT302 potentiostat/galvanostat. Electrochemical synthesis of PPy/GO was performed in 2 $g \cdot L^{-1}$ GO/ 0.2 M Py aqueous solution. Firstly, the synthesis was performed on stainless steel (SS) electrodes employing a three-electrode configuration. When needed, the PPy/GO film was detached for the SS surface with the help of a sharp blade to obtain the membranes. The characteristics of SS electrode plates employed were: (plates of 2 cm × 3 cm × 0.1 cm); the chemical composition in weight (%) was: C ≤0.050, Si 0.750, Mn≤2.000, P 0.040, S 0.015, Cr 18–19, Cu 8.5–9, the rest of the composition corresponds to Fe. Before the electrosynthesis, SS electrodes were degreased with acetone, mechanically polished to obtain a smooth surface and then, cleaned with ultrapure water in an ultrasonic bath. The counter electrode was a SS mesh with cylindrical geometry to equalize the electric field around the working electrode. Electrochemical potential was referred to the Ag/AgCl (3.5 M KCl) reference electrode. Firstly, cyclic voltammetry (CV) technique was employed to determine the synthesis potential (0.86 V was the potential selected). Thereafter, potentiostatic synthesis was performed at 0.86 V until an electrical charge of 1 $C \cdot cm^{-2}$ was achieved.

2.3. Fourier transform infrared spectroscopy with attenuated total reflection (FTIR-ATR)

FTIR-ATR with horizontal mono-rebound attenuated total reflection accessory was performed with a Nicolet 6700 Spectrometer equipped with deuterated triglycine sulfate detector. An accessory with pressure control was used to equalize the pressure in the different solid samples. A prism of ZnSe was used and spectra were collected with a resolution of 4 cm^{-1}, 64 scans were averaged for each sample. GO powders were characterized to assign their different contributions.

2.4. Field emission scanning electron microscopy (FESEM) and energy dispersive X-ray analysis (EDX)

A Zeiss Ultra 55 FESEM was used to observe the morphology of the samples using an acceleration voltage of 3 kV. Energy dispersive X-ray (EDX) measurements were performed between 0 and 10 kV. An optical microscope Zeiss Discovery V.8 was employed to observe the mounting of the membrane on an adhesive tape.

2.5. Electrochemical impedance spectroscopy measurements

A two-electrode configuration was employed to measure the electronic conductivity of the PPy/GO films. The PPy/GO sample was located between two metals; one was the SS electrode where the film was grown and the other was Hg, applied as drops on the surface of the PPy/GO film. Hg is liquid and adapts to the surface topography of the electrode, thus allowing a better interfacial contact with the electrode material than when employing rigid metallic electrodes.

A standard three-electrode design was used to measure the EIS response of SS-PPy/GO electrodes in 0.1 M H_2SO_4 solutions. An asymmetrical configuration metal-sample-electrolyte was used. An Ag/AgCl (3.5 M KCl) electrode and Pt wire were used as reference electrode and counter electrode, respectively.

A four-electrode configuration was employed to measure the transport properties across the PPy/GO free-standing membrane. A two-compartment symmetrical electrochemical cell was employed to carry out the measurements. The membrane separated the two compartments. Two Pt electrodes were employed as auxiliary electrodes and two Ag/AgCl (3.5 M KCl) reference electrodes were employed to measure the potential. The measurements were performed in 0.50 M, 0.10 M, 0.05 M and 0.01 M NaCl solutions. 0.1 M tetramethylammonium solutions were used to test the effect of size of the ion on the diffusion-migration through the membrane.

EIS measurements were performed in the 10^5 to 10^{-2} Hz frequency range by using an Autolab PGSTAT302 potentiostat/galvanostat. The amplitude of the sinusoidal voltage was ± 10 mV. Each measurement was carried out at a constant imposed potential equal to the stabilized open circuit potential at the beginning of the experiment. The experimental results were also fitted using a non-linear least squares fitting minimization method by ZView software (version 2.7).

2.6. Scanning electrochemical microscopy (SECM)

SECM measurements were carried out with a scanning electrochemical microscope of Sensolytics. A three-electrode configuration cell consisting of a 25-µm-diameter Pt microelectrode, a Pt wire auxiliary electrode and an Ag/AgCl (3.5 M KCl) reference electrode. Measurements were performed in 0.01 M $Fe(CN)_6^{3-}$ / 0.1 M KCl and 0.01 M $Ru(NH_3)_6^{3+}$ / 0.1 M KCl solutions. All the experiments were carried out in an inert nitrogen atmosphere after deoxygenation by N_2 bubbling. The samples were glued to microscope slides with epoxy resin. The microelectrode operated at a potential of -0.4 V for $Ru(NH_3)_6^{3+}$, or 0 V for $Fe(CN)_6^{3-}$, at which the oxidized form of the redox mediator (Ox) is reduced (Red) at a diffusion controlled rate. Approach curves were obtained by

recording the tip reduction current as the Pt microelectrode tip was moved in z direction. Approach curves give us an indication of the electroactivity of the surface. These curves were compared to the theoretical positive feedback model. The substrate surface in all the measurements was at its open circuit potential (OCP). 2-D and 3-D representations of the array scans were obtained by positioning the microelectrode inside the influence of the electrochemical field, at a proper height over the substrate surface.

3. Results and discussion

3.1. Electrochemical synthesis

The electrochemical synthesis of PPy/GO on SS electrodes was performed in 0.2 M pyrrole and 2 $g \cdot L^{-1}$ GO aqueous solution. No additional electrolyte was added to the solution to avoid the incorporation of anions arising from the supporting electrolyte as counter ion in the PPy matrix; this approach has been also employed by other authors [11,12,21]. It should be taken into account that GO presents carboxylic acids in its structure, which can release H^+ that act as electrolyte to conduct the charges [22]. Fig. 1-a shows the characterization of the SS electrode in the synthesis solution. As can be seen, the current density increases with the number of scan. It is important to avoid over-oxidation of the polymer, for this reason the potential selected to carry out the synthesis was 0.86 V. This potential was sufficient to allow the formation of the PPy film as it was stated from SEM and FTIR results. Fig. 1-b shows the current density transient curve for the potentiostatic synthesis at 0.86 V of PPy/GO on SS electrode. Occasional N_2 bubbling was applied since precipitation of GO occurred with time, probably due to the adsorption of Py on the surface of GO due interactions such as π-π

interactions, electrostatic interactions, etc. For this reason graphene materials are employed as adsorbents of organic compounds [23]. The synthesis time (approximately 2 h) was so long due to the low conductivity of the media, hence requiring a longer deposition time. The currents obtained in CV or potentiostatic synthesis for the electrochemical synthesis of PPy/GO without additional electrolyte are lower than for the synthesis of PPy employing additional electrolyte [11]. Thus, a longer time of synthesis is required for the synthesis of PPy/GO without adding supporting electrolyte. However, this approach avoids the incorporation of electrolyte anions as counter ions in the structure of PPy as mentioned previously.

3.2. FTIR-ATR characterization

Fig. 2 shows the FTIR-ATR characterization of PPy/GO films. The spectrum of GO powders is also presented as reference. The main peaks observed for GO were: the band at 1720 cm^{-1} which was associated with the stretching vibrations of C=O bonds [24]. The peak at 1613 cm^{-1} was ascribed to C=C skeleton vibration from unoxidized sp^2 bonds [24]. The band at 1220 cm^{-1} was attributed to C-OH stretching vibrations, and finally the band around 1050 cm^{-1} was assigned to C-O stretching vibrations [24].

Afterwards, both sides of the PPy/GO films (the side in contact with the SS electrode and the one in contact with the solution) were characterized to see whether there were differences between them. Different bands attributed to PPy were observed, the most significant were [25]:

- The band around 1540 cm^{-1} which was associated to the pyrrole ring stretching vibration (C=C).
- C-C stretching vibration can be observed at 1450 cm^{-1}.

- The characteristic bands of the bending vibration of pyrrole can be observed at 775, 1037 and 1162 cm^{-1}.
- The band at 1092 cm^{-1} was attributed to the N^{+}-H in plane deformation.
- The band at 956 cm^{-1} was attributed to C-C out of plane deformation.

Regarding GO presence in the PPy/GO films, a band at 1700 cm^{-1} attributed to C=O stretching vibrations appeared in the spectra. This band suffered a displacement when compared with GO powders and it was due to the interaction of GO and PPy (π-π interactions and hydrogen bonding) [11], which confirmed the synthesis of the hybrid material.

Little difference was observed between the two sides of the PPy/GO sheets (the one in contact with the solution and the one in contact with the SS electrode). Only the intensity of the band at 1700 cm^{-1} varied. This could be due to the more planar structure of the side grown on the SS electrode side which would allow a better contact of the film with the ZnSe crystal employed to carry out the measurements. The measurements were performed in triplicate in different parts of the sample and the same tendency was observed for all of them.

3.3. FESEM and EDX

FESEM was employed to observe the morphology of the PPy/GO films. Fig. 3-a shows the micrograph of the side in contact with the SS electrode. It can be seen that the surface is very smooth with no mentionable features (when compared with the other side of the film). Fig. 3-b shows the inner structure of the coating, as can be seen the structure is very porous due to the incorporation of GO sheets during the polymerization of Py to produce PPy. Since no additional electrolyte was employed, the negative charges of GO compensate the positive charges created in the structure of PPy (polarons

and bipolarons). Fig. 3-c shows a magnified micrograph that shows the GO sheets coated with PPy. In Fig. 3-d, a micrograph showing ordered deposition of PPy/GO sheets in a punctual spot is presented, the self-assembly of different PPy/GO sheets was observed. The thickness of the PPy/GO sheets is below 20 nm. However, in general, the deposition was disordered as can be seen in Fig. 3-b and Fig. 3-c.

Fig. 4-a shows the FESEM characterization of the side of the PPy/GO film in contact with the synthesis solution. It can be seen that the morphology is totally different from the side in contact with the SS electrode. This side is rougher and the presence of GO sheets can be easily observed. In the case of the side in contact with the SS electrode it seems that the first step is the PPy polymerization which produced a fine structure. Later, GO sheets were progressively incorporated in the structure of the film as it grows. Fig. 4-b shows a magnified micrograph where the PPy structure can be observed. In Fig. 4-c, a GO sheet can be observed in the center of the image. It can be seen that PPy globules are progressively growing on its surface. Fig. 4-d shows the presence of different GO sheets on the PPy structure. The wrinkles of GO help to locate them [26] on the surface of the PPy/GO coating.

Fig. 5 and Fig. 6 shows the EDX characterization of the PPy/GO film. The elements detected were C, O, N, S and Cl. S and Cl are impurities that arise from the synthesis process of GO that employs sulfuric acid among other strong acids and oxidants. The presence of N indicates the formation of the PPy coating. The presence of O is mainly attributed to GO, although it could also be present in PPy structure due to oxidation of chain structure. Fig. 5 also shows the element map distribution of the major elements. There was a uniform distribution of all the elements on the side in contact with the SS electrode. On the other hand, the side in contact with the solution (Fig. 6) showed the accumulation of C and O in the zones where GO sheets where deposited. Taking into

account the FESEM and EDX data, this would indicate that in the mechanism of film formation, PPy film is firstly formed on the SS electrode and thereafter, GO sheets are progressively incorporated within the growing film. As can be seen in both EDX spectra (Fig. 5-e and Fig. 6-e), significant differences in the composition of both sides of the film were not observed. X-ray are able to penetrate several microns inside the sample and hence a bulk composition is obtained instead of a surface one.

3.4. EIS characterization

EIS technique with the two-electrode configuration was employed to measure the electronic conductivity of the PPy/GO film. The metal-PPy/GO-metal symmetrical configuration was employed for this purpose. Fig. 7 shows the corresponding Nyquist plot obtained. The electrical behavior of the material (black dots) can be modeled as a RC (resistance-capacitor) system. The characteristic frequency for this time constant was 16000 Hz. The electronic resistance for the PPy-GO film was Rf = 107 $\Omega \cdot cm^2$. Considering the thickness of the film, noting Fig. 3-b (~5 μm), the electronic conductivity was $4.7 \cdot 10^{-6}$ S/cm, higher than the value obtained for PPy/$PW_{12}O_{40}^{3-}$ membrane (~$7.5 \cdot 10^{-8}$ S/cm) [7]. The capacitance of the PPy-GO film as dielectric material (without solution) was Cf = $6.3 \cdot 10^{-8}$ F/cm^2.

The four-electrode symmetrical configuration was employed to measure the ion conducting properties through PPy/GO free-standing membrane. First, PPy/GO film was detached from the SS electrode and was mounted between an adhesive tape that had a hole to communicate both sides of the electrochemical cell. Fig. 8-a shows an optical microscope image of the side of the membrane that was grown on the stainless steel electrode. Fig. 8-b shows the side of the membrane that was in contact with the synthesis solution. Since the side in contact with the SS electrode was smoother it

reflects more light than the other side of the membrane, which was rougher and reflects less light. The size of the exposed membrane area was 1.44 mm^2. The electrolyte used was 0.1 M H_2SO_4. Fig. 7 (red dots) shows the Nyquist plot for the symmetrical configuration 0.1 M H_2SO_4/PPy-GO/0.1 M H_2SO_4, i.e. the membrane ionic impedance. The high frequency loop is due to polymer/electrolyte interface. The low frequency loop is due to diffusion-migration of ionic-electronic charge carriers (counter-ions and polarons) [27]. The overall ionic resistance of the membrane has a value of 4 $\Omega \cdot cm^2$.

Once the separate electrical and ionic behavior had been analyzed by the two symmetrical configurations, metal-PPy/GO-metal and solution-PPy/GO-solution, the next step was the analysis of the overall electrical response with a conventional three-electrode cell. Figs. 9-a, and 9-b show the Nyquist and Bode plots for the PPy-GO/SS electrode immersed in 0.1 M H_2SO_4 solution. The high frequency loop (Fig. 9-a) has a characteristic frequency similar (resistance and capacitance also similar) to the electrical response obtained in Fig. 7. Therefore, this time constant is also due to the electronic properties of the PPy/GO film in the asymmetric configuration metal-PPy/GO-solution. The different values were fitted using a non-linear least squares fitting minimization method by ZView software. The electronic resistance for the film was 100 $\Omega \cdot cm^2$ and the corresponding capacity was $9.1 \cdot 10^{-8}$ F/cm^{-2}.

Other relaxation process appears at middle-low frequencies (1-0.01 Hz). Seeing the Bode diagram in Fig. 9-b, a phase angle of about -45º was obtained at 0.01 Hz. This shows in principle Warburg behavior. Taking into account that there are not redox couples in solution, the following equivalent electrical circuit is proposed in the inset of Fig. 9-b. This equivalent circuit is composed of:

- Rs: Electrolyte resistance.
- Rf: Electronic resistance of the PPy/GO film.

- Cf: Capacitance of the PPy/GO film.

- Wd: Warburg impedance due to counter-ion + polaron diffusion-migration. W-R: diffusion-migration resistance. W-T: l^2/D (s), l: length of the diffusion-migration layer, D: binary counter-ion + polaron diffusion-migration coefficient. W-P: Warburg exponent.

The second loop at low frequencies is due to diffusion-migration process. Migration-diffusion resistance is about 11 $\Omega \cdot cm^2$ (4 $\Omega \cdot cm^2$ for ionic symmetric configuration in Fig.7, and 13 $\Omega \cdot cm^2$ for dc resistance of the membrane in section 3.5). Therefore, the rate-determining step is the low electronic conductivity of the PPy/GO film (100 $\Omega \cdot cm^2$).

3.4.1. EIS response of PPy/GO free-standing films in NaCl solutions of different concentration and $(CH_3)_4N^+Cl^-$

The PPy/GO free-standing film was placed in a symmetrical configuration between two ionic solutions and an ac voltage was applied. The electrical response is due to the following phenomena [19]:

- Re: Electrolyte resistance

- Zi: Ion transfer impedance at the polymer/electrolyte interface.

- Zp: Ion transport impedance within the film.

The physical phenomena of PPy free-standing films may be modeled according to the equivalent circuit [19] showed in Fig. 10.

To study the electric properties of the PPy/GO membranes in relation to electrolyte concentration, four different NaCl solutions were prepared with the following concentrations: 0.01, 0.05, 0.10 and 0.50 M. To see the effect of the size of the ion on the ion diffusion, a 0.10 M tetramethylammonium chloride solution was also prepared

and tested. Fig. 11 shows the Nyquist plot for a PPy-GO membrane immersed in 0.1 M NaCl solution with the symmetrical configuration. Two loops appeared in the diagram due to two relaxation processes. The high-middle frequencies loop is related to the ionic exchange between PPy/GO membrane and the solution. The diagram shows a second loop at low frequencies. This time constant is due to the counter-ion diffusion in the bulk polymeric film. This diffusion presented transmissive boundary conditions, since a resistive behavior at very low frequencies is shown in the Nyquist plot, typical in this ion non-blocking interface.

Fig. 12 shows the Bode plots for PPy/GO membrane that was immersed in NaCl and tetramethylammonium chloride solutions with different concentrations: 0.01, 0.05, 0.10 and 0.50 M. Nyquist plots are not shown because the shape was very similar to Fig. 11. Two time constants can be appreciated in the plot phase vs. frequency for all the assays. The high-middle frequency range (10,000–1 Hz) corresponds to the ionic exchange impedance between membrane and solution, as it was commented before. This time constant changed to lower frequencies when the NaCl solution was more diluted. The middle-low frequency range (1–0.01 Hz) is due to diffusion-migration of counter-ions in the polymeric membrane. The time constant changed to lower frequencies when the NaCl solution was more diluted. Seeing the impedance modulus vs. frequency plot, the impedance modulus increased when the membrane was immersed in more diluted solutions for all the frequencies analyzed. Therefore, the two relaxation processes (ionic exchange impedance and diffusion-migration of counter-ions within the membrane) were slower when the NaCl concentration was lower.

To analyze the effect of the electrolyte ions size, the PPy-GO membrane was immersed in 0.10 M $(CH_3)_4N^+Cl^-$ solution. Bode plots in Fig. 12 show how both, ionic exchange and diffusion-migration presented a similar behavior for 0.1 M $(CH_3)_4N^+Cl^-$ solution in

comparison to 0.1 M NaCl one. The trimethylammonium ion size is much larger than chloride and sodium ions. This fact confirms the high porosity of the PPy/GO films as it was discussed in section 3.3 (Fig. 3-b).

3.5. Cyclic voltammetry characterization

Cyclic voltammetry was also performed in 0.5 M H_2SO_4 solution with and without the membrane using the 4-electrode configuration (Fig. 13). The voltammograms showed a linear resistive response. The slope of the voltammogram without the membrane was related to the resistance of the electrolyte and the electrode configuration employed; the calculated resistance was 60 Ω. When the PPy/GO membrane was located, there was a decrease of the current intensity measured, indicating an increase of the resistance due to the presence of the membrane. The calculated dc resistance of the membrane after subtracting the electrochemical configuration was 13 Ω. Taking into account the thickness of the membrane (5 μm) and the membrane area (1.44 mm^2), the ionic dc (direct current) conductivity of the PPy-GO membrane was: $1.6 \cdot 10^{-3}$ S/cm. This value is two orders of magnitude higher than in previous work for PPy/$PW_{12}O_{40}^{3-}$ membrane ($1.7 \cdot 10^{-5}$ $S \cdot cm^{-1}$) [7].

Taking into account the high porosity obtained that enhances the ion conductivity through the membrane, the high surface area and the conductivity of the composite material there are several applications where these materials can be used. One of them is the electroanalysis of heavy metals, where the high surface area and functional groups of GO and PPy help in the processes of pre-concentration and stripping of metal ions [28-30]. The 3-D architecture obtained helps in enhancing the surface area which is beneficial for different purposes such as adsorption, detection, etc. [31]. The incorporation of metal nanoparticles inside this 3-D structure has not been reported and

would be advantageous for the electroanalysis of heavy metals. The high porosity of the PPy/GO hybrid material shows that the size of the counter ion has no effect on the ionic diffusion-migration, which would allow the easy adsorption of metal precursors ($AuCl^{4-}$, $PtCl_6^{2-}$, Ag^{+}, etc.) inside the 3-D structure. Thereafter, these precursors would be reduced to metal nanoparticles chemically or electrochemically (given that the composite material is electrically conducting). Other possible approach is to perform the synthesis of the nanoparticles and PPy/GO simultaneously. The synergies provided by PPy, GO and metal nanoparticles would produce sensors with decreased limit of detection. Other applications, if Pt nanoparticles were to be synthesized, include electrode material for fuel cells (methanol or ethanol oxidation) [32], etc. More work is in progress to evaluate the application of these materials. The mechanical stability of the PPy/GO hybrid material as a free-standing membrane is limited due to its highly porous structure and low thickness of the film, although when supported on an electrode material is good. In order to increase the mechanical stability of the free-standing film, one approach that can be employed is the use of higher synthesis charges to obtain thicker films. Values of up to 5 $C \cdot cm^{-2}$ have been reported in bibliography with the outcome of good mechanical properties [11]. For the different applications mentioned previously, the hybrid material will be used as a deposited film on a supporting electrode, which allows the electron transfer. Different supporting materials are being studied at present for this purpose.

3.6. SECM characterization

SECM was employed to test the electroactivity of the PPy/GO films. The characterization by SECM of PPy/GO films obtained electrochemically has not been reported in bibliography and only our previous work dealt with the SECM

characterization of PPy/GO obtained chemically [25]. Few works have applied this technique to study graphene materials [22,24,26,33-37]. SECM is a powerful technique that can be employed to measure the electroactivity [22,24,26,34,36], electron transfer kinetics [33,35] or even conductivity [37] of graphene materials. The technique was operated in the feedback mode which is based on measuring the current on the surface of a microelectrode as the microelectrode approaches the surface of the substrate subject of study [34]. Fig. 14-a shows the approach curves obtained employing PPy/GO film supported on SS electrode as substrate. Two different redox mediators were employed ($Fe(CN)_6^{3-}$ and $Ru(NH_3)_6^{3+}$). For both redox mediators, positive feedback was obtained. The behavior was very close to the ideal positive feedback of a conducting material.

The positive feedback model curve was obtained according to equation 1. According to Rajendran el al. [38], Pade's approximation gives a close and simple equation with less relative error for all distances and is valid for RG > 10. The approximate formula of the steady-state normalized current assuming positive feedback for finite conductive substrate together with finite insulating glass thickness is:

$$I_T{}^C = \left[\frac{1 + 1.5647/L + 1.316855/L^2 + 0.4919707/L^3}{1 + 1.1234/L + 0.626395/L^2} \right] \quad (1)$$

The membrane was detached from the SS electrode and was also analyzed to discard any contribution for the metallic substrate. In this case, only the $Fe(CN)_6^{3-}$ redox mediator was employed to carry out the measurements since similar response was obtained for both redox mediators. As can be seen in Fig. 14-b the PPy/GO membrane shows also positive feedback close to the ideal conducting behavior. Both sides of the membrane were analyzed (the one in contact with the SS electrode and the one in contact with the solution). Similar behavior was obtained for both sides of the PPy/GO membrane analyzed, indicating a similar electroactivity degree for both sides. The

degree of positive feedback and the adjust to the theoretical model for positive feedback was superior for PPy/GO electrochemically obtained than when PPy/GO composites were obtained chemically [25]. This indicates a higher electroactivity of PPy/GO synthesized electrochemically.

Fig. 15 shows the 2-D and 3-D representations of PPy/GO supported on SS electrode. As can be seen, the values of normalized current are between 1.26 and 1.58 (within the positive feedback zone). This indicates a homogeneous distribution of the conducting material. The variations in the value of positive feedback can be attributed to the variations in morphology and topography observed in the side in contact with the solution, as observed in micrographs of Fig. 4.

4. Conclusions

PPy/GO coatings were obtained on stainless steel electrodes by potentiostatic synthesis. FTIR-ATR showed the formation of the hybrid material and the effective incorporation of GO in the structure. As observed by FESEM, the structure of the coating was very porous due to the incorporation of GO that was intercalated in the PPy structure. Differences in morphology between the side grown on the stainless steel electrode and the side in contact with the solution were observed. It seems that the first stage is the formation of a PPy film and progressively GO sheets are incorporated within the coating.

Conductivity of the films was studied by EIS with the symmetric metal-PPy/GO-metal configuration and the electronic conductivity obtained was $4.7 \cdot 10^{-6}$ S/cm. The measurement with the asymmetrical metal-PPy/GO-solution configuration showed the appearance of two time constants attributed to the electron transport and the diffusion-

migration processes. The rate-determining step was the electronic transport in the PPy/GO film. The transport study across PPy/GO free standing film acting as a membrane was analyzed by means of EIS in solution with the solution-PPy/GO-solution configuration. The ionic dc conductivity of the PPy/GO membrane was $1.6 \cdot 10^{-3}$ S/cm. PPy/GO membranes are excellent ionic conductors due to its high porosity. No difference was observed when employing different size ions for the study of ion diffusion, which indicates that the pore size is high enough to allow differences to be observed. Due to the good diffusion-migration properties of the material, its conductivity and high surface area, it can be used for electrochemical applications such as sensors or as a support to deposit other catalytic materials for electrochemical applications.

SECM technique showed that the material was electroactive and behaved like an ideal conductor showing positive feedback. The 2-D and 3-D mapping of surface electroactivity showed a homogeneous distribution of the material.

Role of the funding source

The funding sources had no involvement in the study design; in the collection, analysis and interpretation of data; in the writing of the report; and in the decision to submit the article for publication.

Acknowledgements

Authors wish to thank to the Spanish Ministerio de Ciencia e Innovación (contract CTM2011-23583) for the financial support. J. Molina is grateful to the Conselleria

d'Educació, Formació i Ocupació (Generalitat Valenciana) for the Programa VALi+D Postdoctoral Fellowship (APOSTD/2013/056). A.I. del Río is grateful to the Spanish Ministerio de Ciencia y Tecnología for her FPI fellowship. Electron Microscopy Service of the UPV (Universitat Politècnica de València) is gratefully acknowledged for help with FESEM and EDX characterization.

References

[1] M. Ates, T. Karazehira, A.S. Sarac, Conducting polymers and their applications, Curr. Phys. Chem. 2 (2012) 224-240.

[2] K.S. Novoselov, A.K. Geim, S.V. Morozov, D. Jiang, Y. Zhang, S.V. Dubonos, I.V. Grigorieva, A.A. Firsov, Electric field effect in atomically thin carbon films, Science 306 (2004) 666-669.

[3] K.S. Novoselov, V.I. Fal'ko, L. Colombo, P.R. Gellert, M.G. Schwab, K.Kim, A roadmap for graphene, Nature 490 (2012) 192-200.

[4] S. Park, R.S. Ruoff, Chemical methods for the production of graphenes, Nat. Nanotechnol. 4 (2009) 217-224.

[5] S. Pei, H.-M. Cheng, The reduction of graphene oxide, Carbon 50 (2012) 3210-3228.

[6] J. Molina, A.I. del Río, J. Bonastre, F. Cases, Chemical and electrochemical polymerisation of pyrrole on polyester textiles in presence of phosphotungstic acid, Eur. Polym. J. 44 (2008) 2087-2098.

[7] J. Bonastre, J. Molina, J.C. Galván, F. Cases, Characterization of polypyrrole/phosphotungstate membranes by electrochemical impedance spectroscopy, Synth. Met. 187 (2014) 37-45.

[8] D.R. Dreyer, S. Park, C.W. Bielawski, R.S. Ruof, The chemistry of graphene oxide, Chem. Soc. Rev. 39 (2010) 228-240.

[9] G.G. Wallace, R.B. Kaner, M. Muller, S. Gilje, D. Li, Processable aqueous dispersions of graphene nanosheets, Nat. Nanotechnol. 4 (2009) 25-29.

[10] J. Molina, J. Fernández, A.I. del Río, R. Lapuente, J. Bonastre, F. Cases, Stability of conducting polyester/polypyrrole fabrics in different pH solutions. Chemical and electrochemical characterization, Polym. Degrad. Stab. 95 (2010) 2574-2583.

[11] C.Z. Zhu, J.F. Zhai, D. Wen, S.J. Dong, Graphene oxide/polypyrrole nanocomposites: one-step electrochemical doping, coating and synergistic effect for energy storage, J. Mater. Chem. 22 (2012) 6300-6306.

[12] H.-H. Chang, C.-K. Chang, Y.-C. Tsai, C.-S. Liao, Electrochemically synthesized graphene/polypyrrole composites and their use in supercapacitor, Carbon 2 (2012) 2331-2336.

[13] Z. Lv, Y. Chen, H. Wei, F. Li, Y. Hu, C. Wei, C. Feng, One-step electrosynthesis of polypyrrole/graphene oxide composites for microbial fuel cell application, Electrochim. Acta 111 (2013) 366-373.

[14] S.P. Lim, A. Pandikumar, Y.S. Lim, N.M. Huang, H.N. Lim, In-situ electrochemically deposited polypyrrole nanoparticles incorporated reduced graphene oxide as an efficient counter electrode for platinum-free dye-sensitized solar cells, Sci. Rep. 4 (2014) 5305.

[15] S. Li, X. Lu, Y. Xue, J. Lei, T. Zheng, C. Wang, Fabrication of polypyrrole/graphene oxide composite nanosheets and their applications for Cr(VI) removal in aqueous solution, J. Mater. Chem. 22 (2012) 6300-6306.

[16] C. Ehrenbeck, K. Jüttner, S. Ludwig, G. Paasch, The electrochemical impedance of a free-standing polypyrrole membrane, Electrochim. Acta 43 (1998) 2781-2789.

[17] C. Ehrenbeck, K. Jüttner, Ion conductivity and permselectivity measurements of polypyrrole membranes at variable states of oxidation, Electrochim. Acta 41 (1996) 1815-1823.

[18] C. Deslouis, T. El Moustafid, M.M. Musiani, B. Tribollet, Mixed ionic-electronic conduction of a conducting polymer film. AC impedance study of polypyrrole, Electrochim. Acta 41 (1996) 1343-1349.

[19] C. Deslouis, M.M. Musiani, B. Tribollet, Free-standing membranes for the study of electrochemical reactions occurring at conducting polymer/electrolyte interfaces, J. Phys. Chem. 100 (1996) 8994-8999.

[20] http://www.nanoinnova.com/Product/Details/24. Last accessed 08.04.2016.

[21] W. Liu, Y. Fang, P. Xu, Y. Lin, X. Yin, G. Tang, M. He, Two-step electrochemical synthesis of polypyrrole/reduced graphene oxide composites as efficient Pt-free counter electrode for plastic dye-sensitized solar cells, ACS Appl. Mater. Interfaces 6 (2014) 16249-16256.

[22] J. Molina, J. Fernández, A.I. del Río, J. Bonastre, F. Cases, Synthesis of Pt nanoparticles on electrochemically reduced graphene oxide by potentiostatic and alternate current methods, Mater. Charact. 89 (2014) 56-68.

[23] F. Perreault, A.F. de Faria, M. Elimelech, Environmental applications of graphene-based nanomaterials, Chem. Soc. Rev. 44 (2015) 5861-5896.

[24] J. Molina, J. Fernandez, J.C. Ines, A.I. del Rio, J. Bonastre, F. Cases, Electrochemical characterization of reduced graphene oxide-coated polyester fabrics, Electrochim. Acta 93 (2013) 44-52.

[25] J. Molina, A. Zille, J. Fernández, A.P. Souto, J. Bonastre, F. Cases, Conducting fabrics of polyester coated with polypyrrole and doped with graphene oxide, Synth. Met. 204 (2015) 110-121.

[26] J. Molina, J. Fernández, A.I. del Río, J. Bonastre, F. Cases, Chemical and electrochemical study of fabrics coated with reduced graphene oxide, Appl. Surf. Sci. 279 (2013) 46-54.

[27] C. Deslouis, M.M. Musiani, B. Tribollet, M.A. Vorotyntsev, Comparison of the AC impedance of conducting polymer films studied as electrode-supported and freestanding membranes, J. Electrochem. Soc. 142 (1995) 1902-1908.

[28] Z.-Q. Zhao, X. Chen, Q. Yang, J.-H. Liu, X.-J. Huang, Selective adsorption toward toxic metal ions results in selective response: electrochemical studies on a polypyrrole/reduced graphene oxide nanocomposite, Chem. Commun. 48 (2012) 2180-2182.

[29] R. Seenivasan, W.-J. Chang, S. Gunasekaran, Highly sensitive detection and removal of lead ions in water using cysteine-functionalized graphene oxide/polypyrrole nanocomposite film electrode, ACS Appl. Mater. Interfaces 7 (2015) 15935-15943.

[30] Z.-Q. Zhao, X. Chen, Q. Yang, J.-H. Liu, X.-J. Huang, Beyond the selective adsorption of polypyrrole-reduced graphene oxide nanocomposite toward Hg^{2+}: Ultra-sensitive and -selective sensing Pb^{2+} by stripping voltammetry, Electrochem. Commun. 23 (2012) 21-24.

[31] Y. Shen, Q. Fang, B. Chen, Environmental applications of three-dimensional graphene-based macrostructures: Adsorption, transformation, and detection, Environ. Sci. Technol. 49 (2015) 67-84.

[32] W. Zhao, X. Zhou, Z. Xue, B. Wu, X. Liu, X. Lu, Electrodeposition of platinum nanoparticles on polypyrrole-functionalized graphene, J. Mater. Sci. 48 (2013) 2566-2573.

[33] J.-H. Zhong, J. Zhang, X. Jin, J.-Y. Liu, Q. Li, M.-H. Li, W. Cai, D.-Y. Wu, D. Zhan, B. Ren, Quantitative correlation between defect density and heterogeneous

electron transfer rate of single layer graphene, J. Am. Chem. Soc. 136 (2014) 16609-16617.

[34] J. Molina, J. Fernández, C. García, A.I. del Río, J. Bonastre, F. Cases. Electrochemical characterization of electrochemically reduced graphene coatings on platinum. Electrochemical study of dye adsorption, Electrochim. Acta 166 (2015) 54-63.

[35] C. Tan, J. Rodríguez-López, J.J. Parks, N.L. Ritzert, D.C. Ralph, H.D. Abruña, Reactivity of monolayer chemical vapor deposited graphene imperfections studied using scanning electrochemical microscopy, ACS Nano 6 (2012) 3070-3079.

[36] S. Rapino, E. Treossi, V. Palermo, M. Marcaccio, F. Paolucci, F. Zerbetto, Playing peekaboo with graphene oxide: a scanning electrochemical microscopy investigation, Chem. Commun. 50 (2014) 13117-13120.

[37] J. Azevedo, C. Bourdillon, V. Derycke, S. Campidelli, C. Lefrou, R. Cornut, Contactless surface conductivity mapping of graphene oxide thin films deposited on glass with scanning electrochemical microscopy, Anal. Chem. 85 (2013) 1812-1818.

[38] L. Rajendran, S.P. Ananthi, Analysis of positive feedback currents at the scanning electrochemical microscope, J. Electroanal. Chem. 561 (2004) 113-118.

Figure captions

Fig. 1. Electrochemical synthesis of PPy/GO on stainless steel electrodes in 2 $g \cdot L^{-1}$ GO and 0.2 M pyrrole solution. a) Cyclic voltammetry synthesis. b) Current density transient curve for potentiostatic synthesis. Start potential: 0 V, synthesis potential: 0.86 V, Q = 1 $C \cdot cm^{-2}$.

Fig. 2. FTIR-ATR spectra of GO powders and PPy/GO film electrochemically synthesized. The two sides of the PPy/GO film (the side in contact with the stainless steel electrode and the one in contact with the synthesis solution were analyzed). Measured with monorebound ZnSe prism, resolution 4 cm^{-1}, 64 scans.

Fig. 3. FESEM micrographs of PPy/GO film (side corresponding to the stainless steel interface) (a) (x 0.5 K), (b) (x 10 K), (c) (x 18.6 K), (d) (x 185 K).

Fig. 4. FESEM micrographs of PPy/GO film (side corresponding to the electrolyte interface) (a) (x 0.5 K), (b) (x 20 K), (c) (x 20 K), (d) (x 20 K).

Fig. 5. a) SEM micrograph, b) C, c) O and d) N distribution element maps, e) EDX spectra of PPy/GO film, side in contact with the stainless steel electrode. Acquisition time: 100 s.

Fig. 6. a) SEM micrograph, b) C, c) O and d) N distribution element maps, e) EDX spectra of PPy/GO film, side in contact with the stainless steel electrode. Acquisition time: 100 s.

Fig. 7. Nyquist plots for (•) symmetrical configuration metal/PPy-GO/metal and (⁻) fitting of experimental data, exposed electrode area, 1 cm^2, (•) symmetrical configuration 0.1 M H_2SO_4/PPy-GO/0.1 M H_2SO_4 (inset: magnified zone). Exposed electrode area, 1.44 mm^2. Frequency range from 10^5 to 10^{-2} Hz.

Fig. 8. Optical microscope image of the two sides of the PPy/GO membrane located between an adhesive tape. a) Side in contact with the stainless steel electrode, b) Side in contact with the synthesis solution.

Fig. 9. a) Nyquist and b) Bode plots for (•) asymmetrical configuration metal-PPy/GO-0.1 M H_2SO_4 and (–) fitting of experimental data. Frequency range from 10^5 to 10^{-2} Hz. Exposed electrode area, 1 cm^2.

Fig. 10. Electrical circuit for PPy/GO free-standing films in symmetrical configuration solution/membrane/solution.

Fig. 11. Nyquist plots for PPy/GO membrane in 0.1 M NaCl solution. Exposed membrane area: 1.44 mm^2. Frequency range from 10^4 to 10^{-2} Hz. (•) Experimental data. (–) Fitting data. Inset: Electrical circuit for PPy/GO free-standing films in symmetrical configuration solution/membrane/solution.

Fig. 12. Bode plots for PPy/GO membrane in 0.01, 0.05, 0.1 and 0.5 M NaCl, and 0.1 M $(CH_3)_4N^+Cl^-$ solutions. Exposed membrane area: 1.44 mm^2. Frequency range from 10^4 to 10^{-2} Hz.

Fig. 13. Cyclic voltammograms obtained in a 4-electrode arrangement in 0.5 M H_2SO_4 solution, scan rate 50 $mV \cdot s^{-1}$. Obtained without PPy/GO and with PPy/GO membrane. Exposed membrane area 1.44 mm^2.

Fig. 14. Approaching curves for a) PPy/GO deposited on stainless steel, b) PPy/GO membrane detached from the stainless steel electrode. The theoretical positive feedback model has been included as a continuous black line. The redox mediators employed were $Fe(CN)_6^{3-}$ in 0.1 M KCl, and $Ru(NH_3)_6^{3+}$ in 0.1 M KCl. Approaching curves obtained with a 25 μm diameter Pt tip. The tip potentials were 0 V and -0.4 V for $Fe(CN)_6^{3-}$ and $Ru(NH_3)_6^{3+}$, respectively. The approach rate was 20 $\mu m \cdot s^{-1}$. The area employed was 0.7 cm^2 for a) and 10 mm^2 for b).

Fig. 15. 2-D (a) and 3-D (b) constant height SECM images of PPy/GO on SS electrode. 0.7 cm^2 geometrical area sample, images were taken with a 25 μm diameter microelectrode, in 0.01 M $Fe(CN)_6^{3-}$ and 0.1 M KCl at a constant height of 20 μm. The tip potential was 0 V, the scan rate was 50 $\mu m \cdot s^{-1}$ in comb mode; lengths of x and y lines were 200 μm x 200 μm with increments of 10 μm.

Figure 1

Click here to download high resolution image

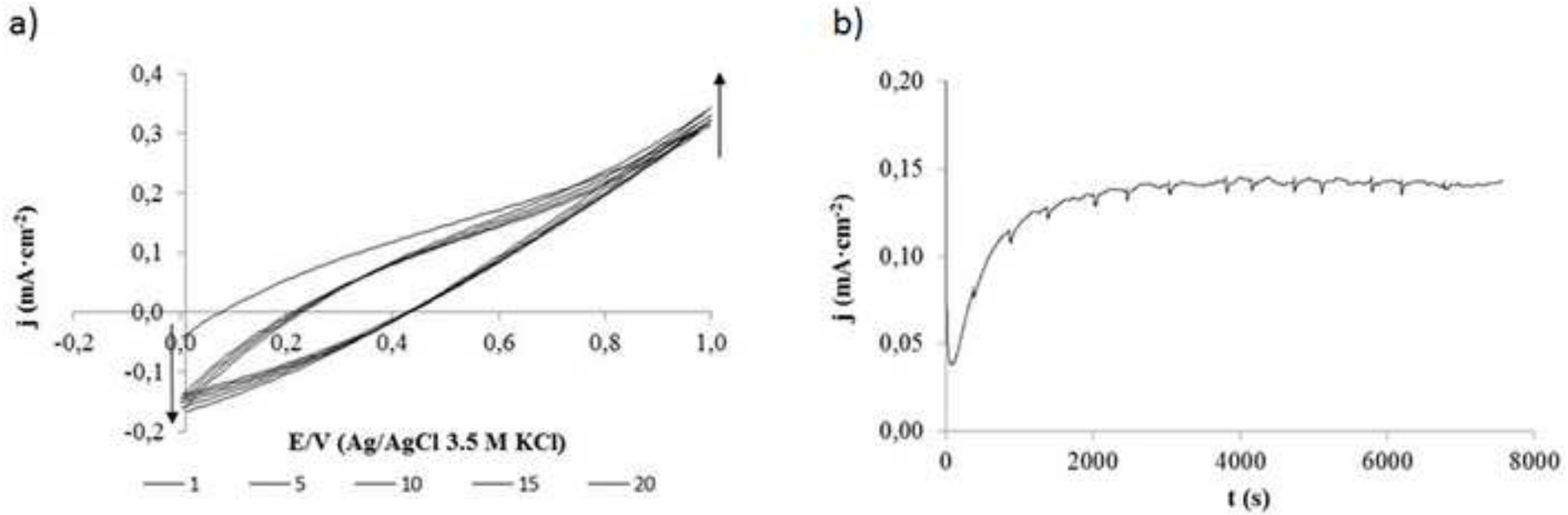

Figure 2

Click here to download high resolution image

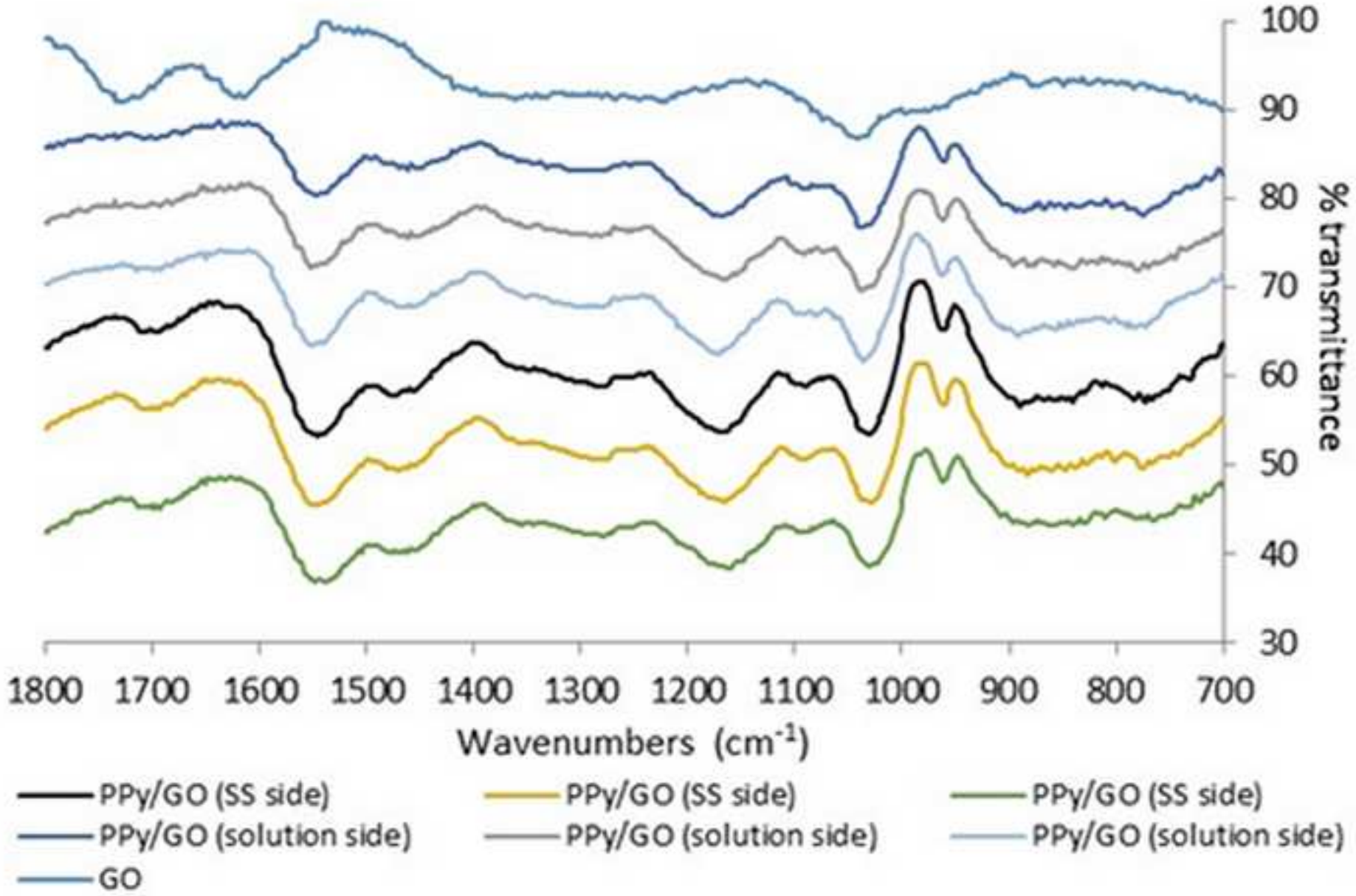

Figure 3

Click here to download high resolution image

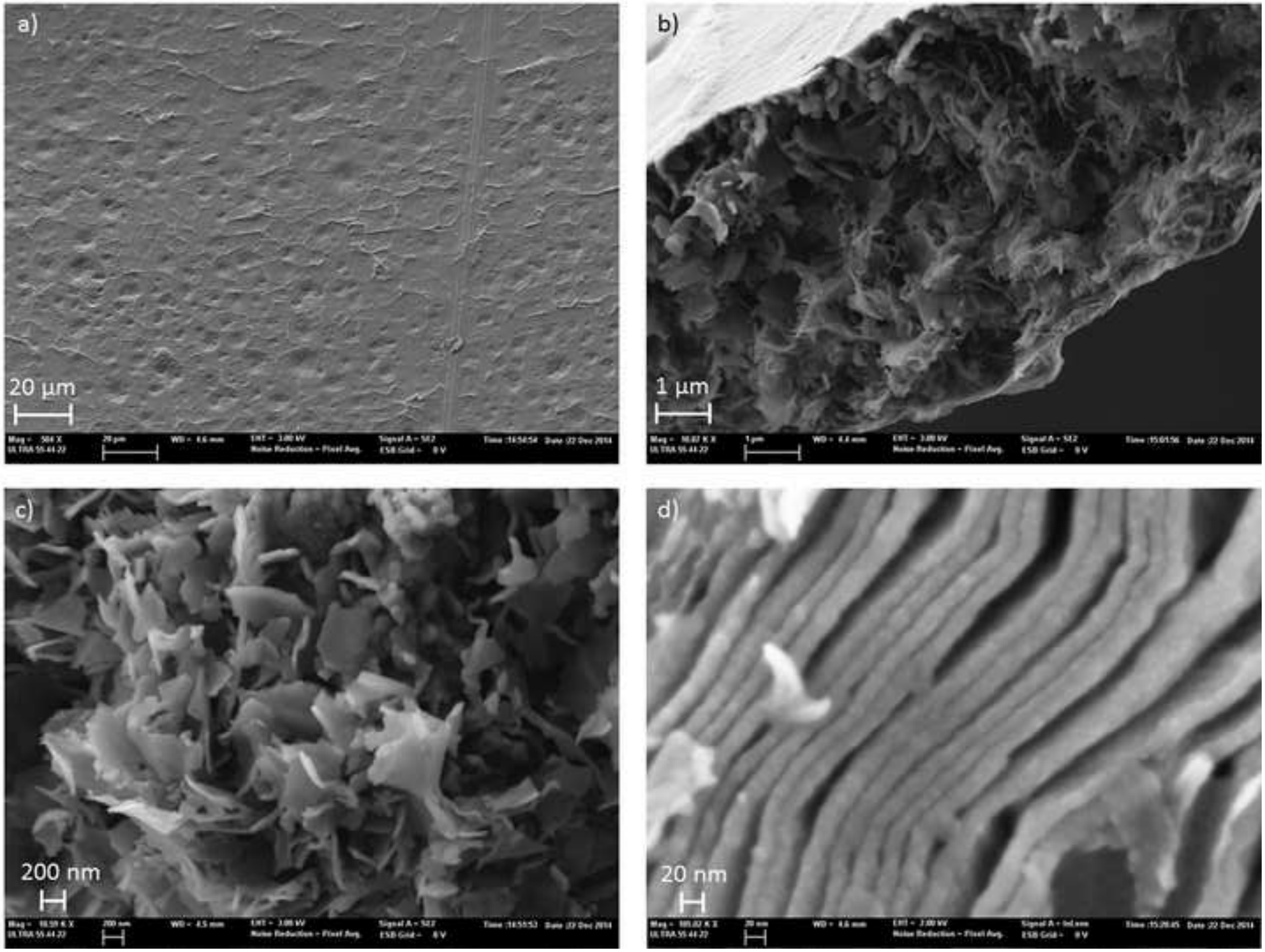

Figure 4

Click here to download high resolution image

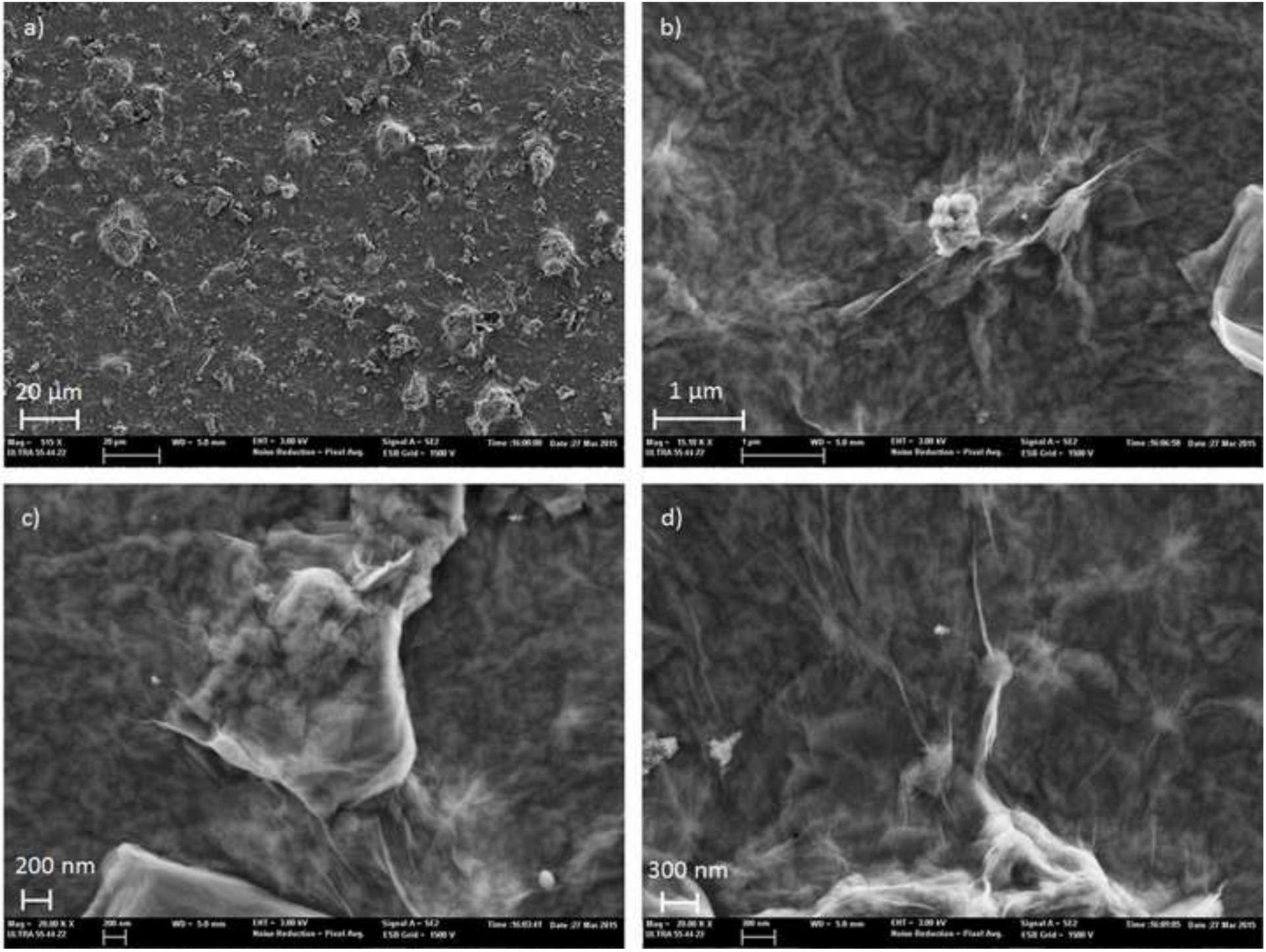

Figure 5

Click here to download high resolution image

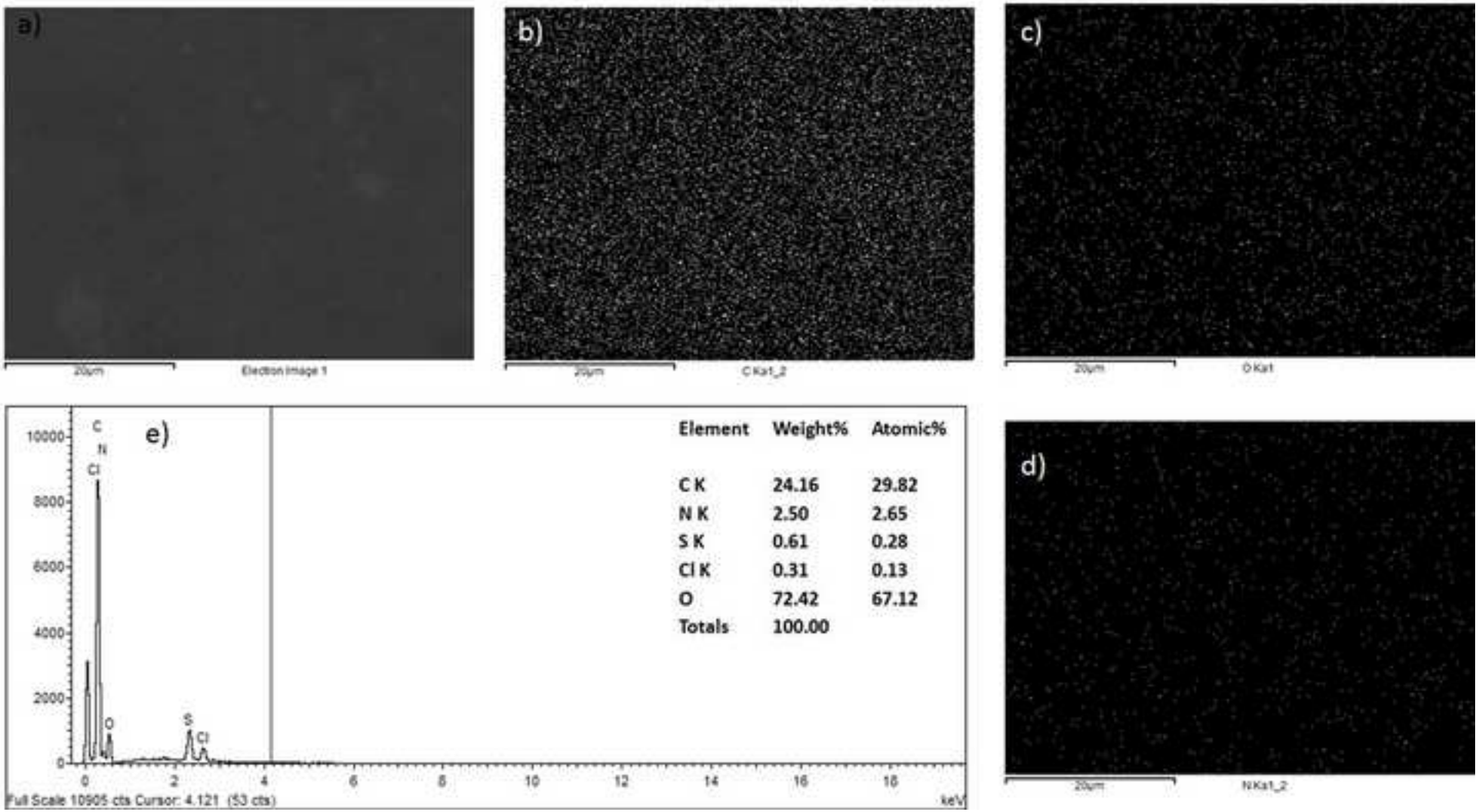

Element	Weight%	Atomic%
C K	24.16	29.82
N K	2.50	2.65
S K	0.61	0.28
Cl K	0.31	0.13
O	72.42	67.12
Totals	100.00	

Figure 6

Click here to download high resolution image

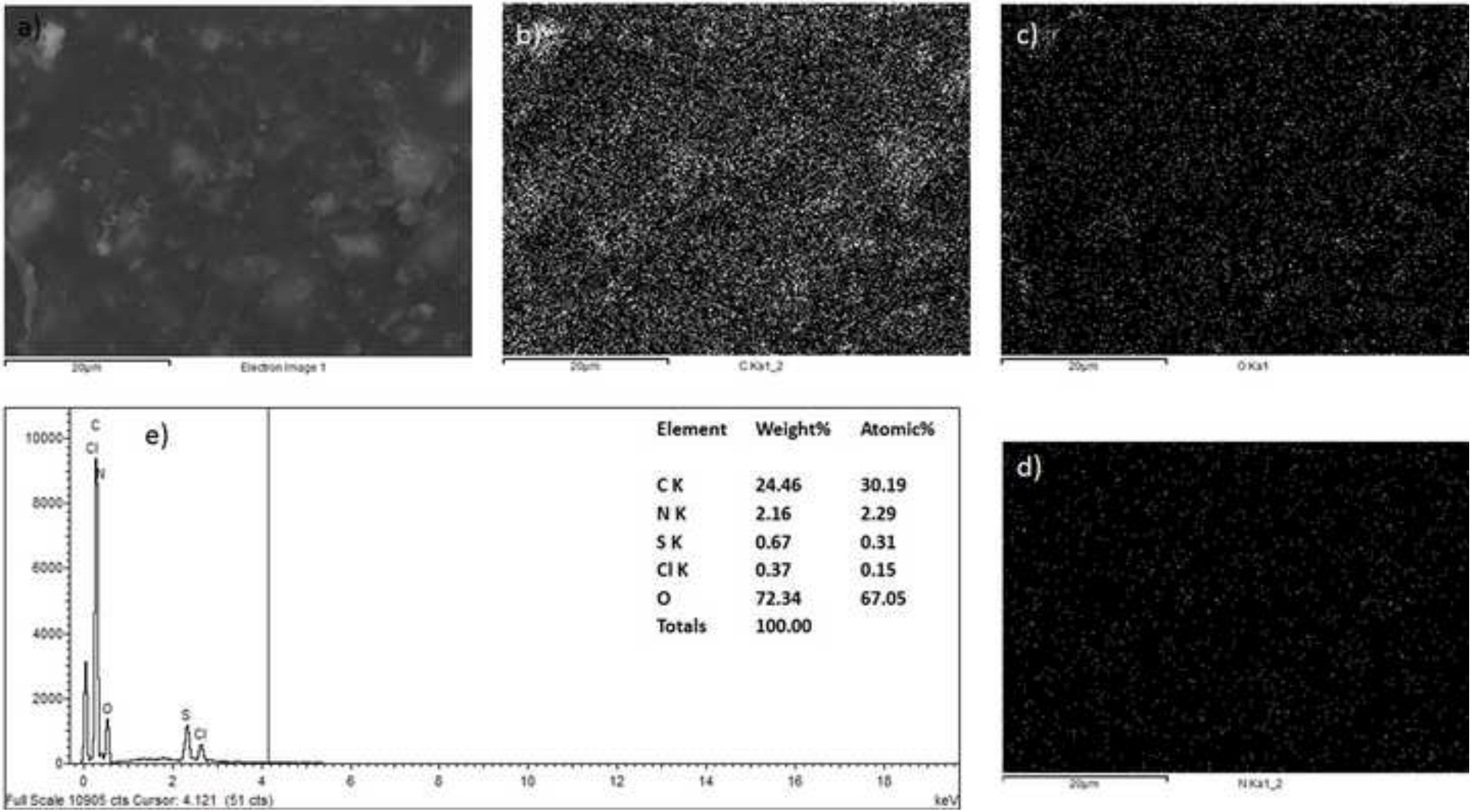

Figure 7

Click here to download high resolution image

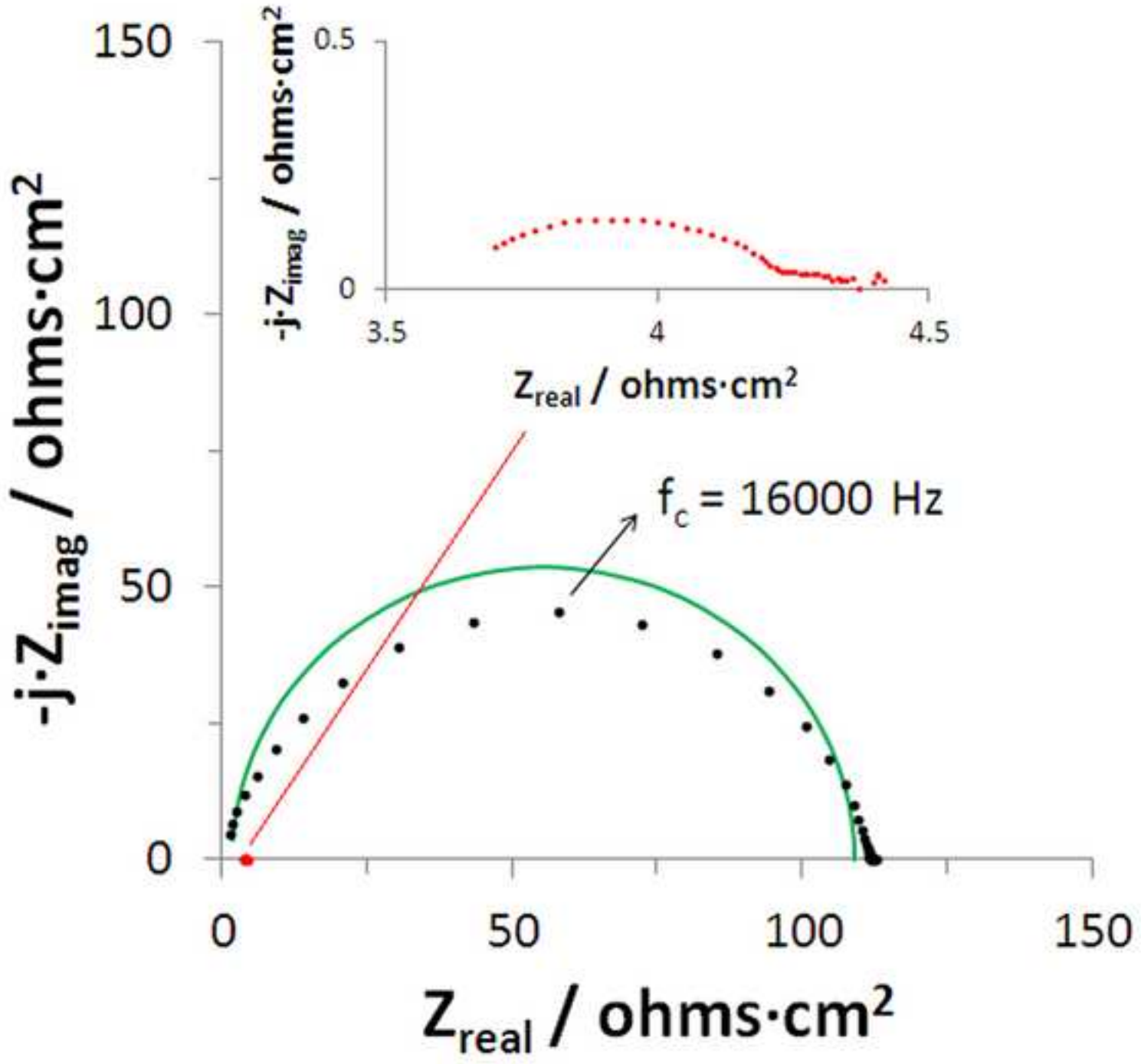

Figure 8

Click here to download high resolution image

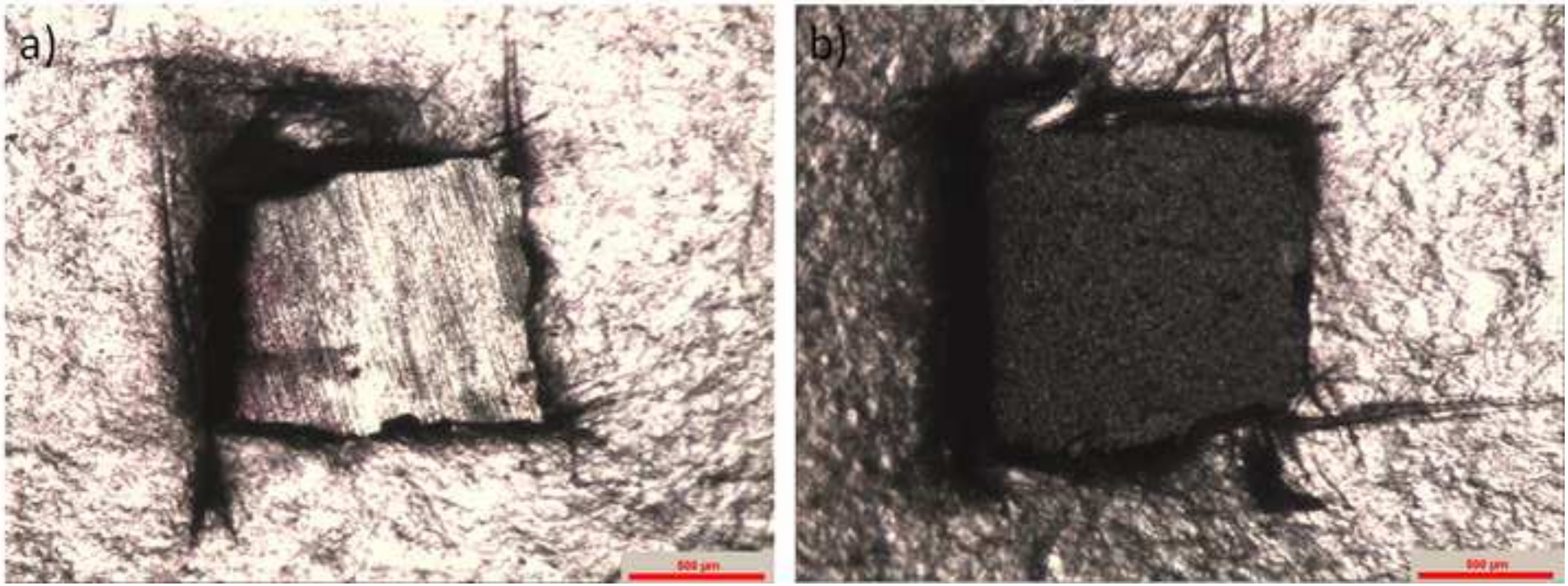

Figure 9

Click here to download high resolution image

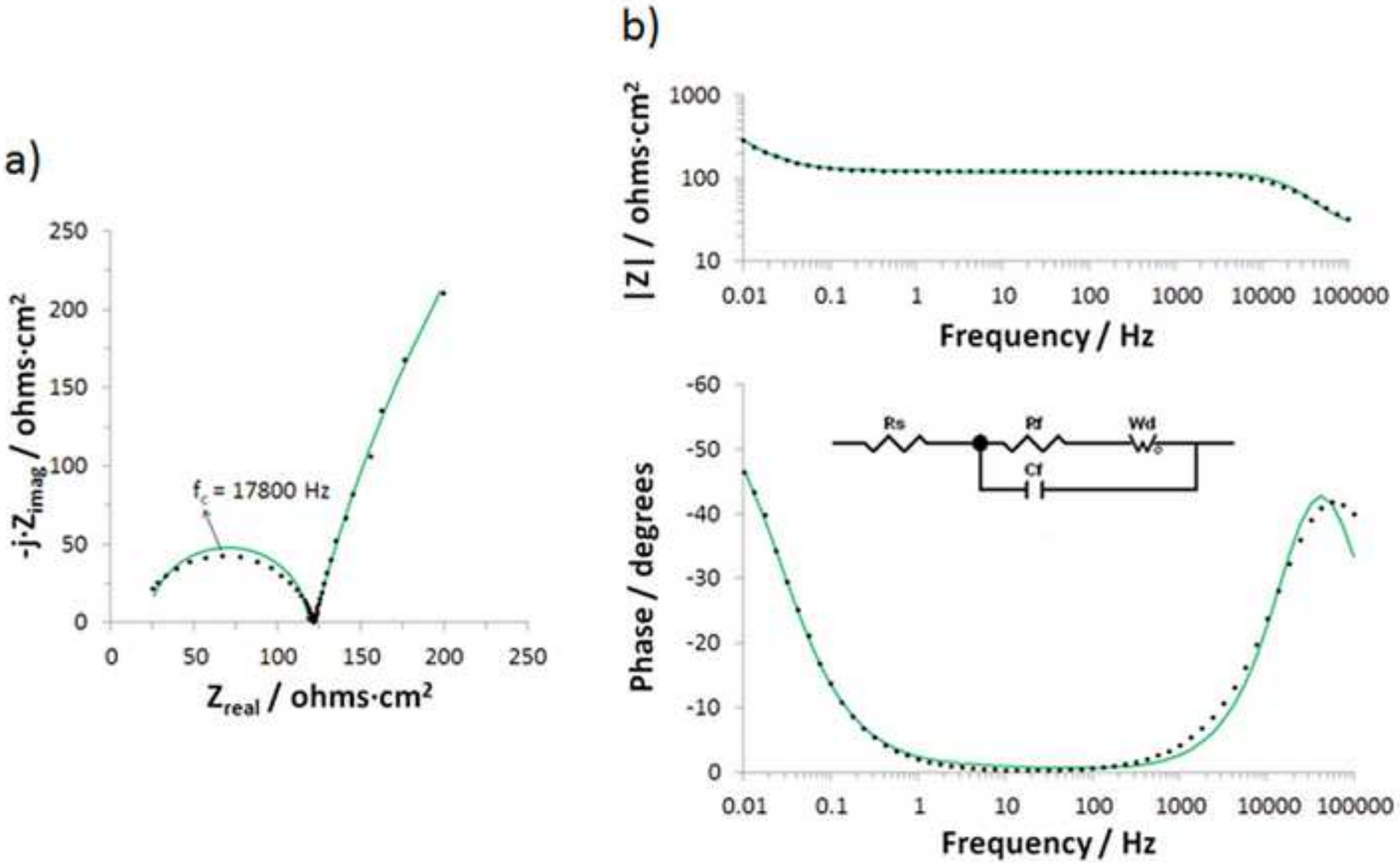

Figure 10

Click here to download high resolution image

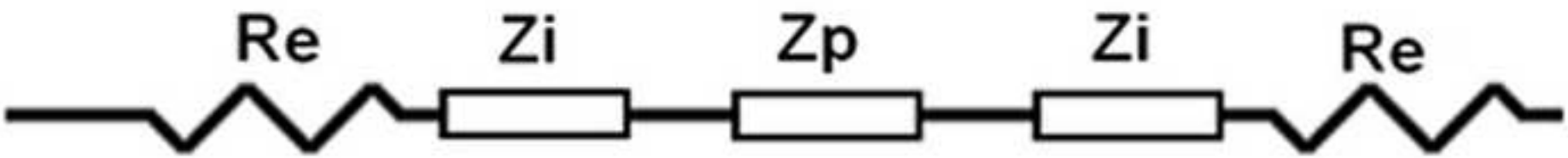

Figure 11

Click here to download high resolution image

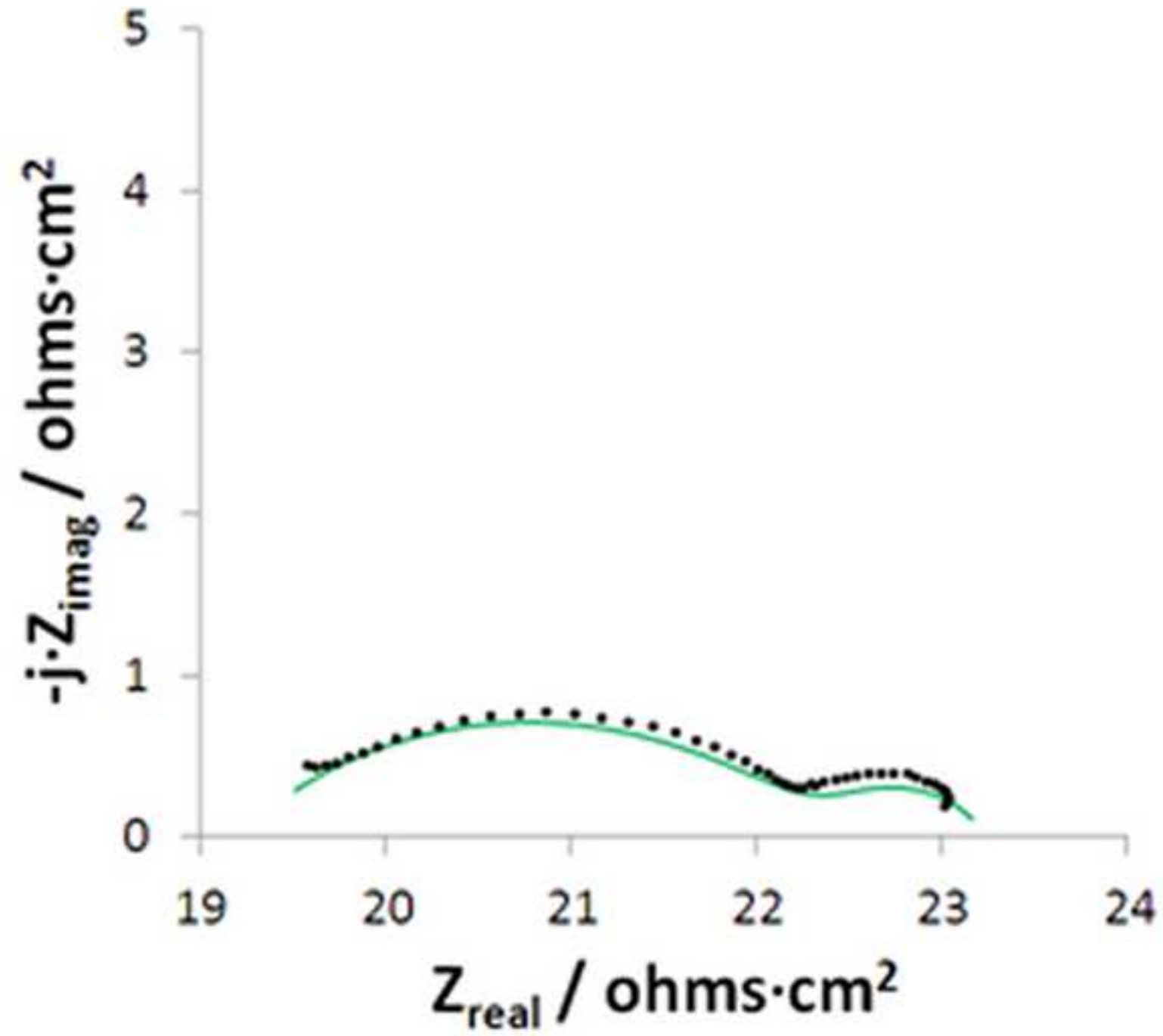

Figure 12

Click here to download high resolution image

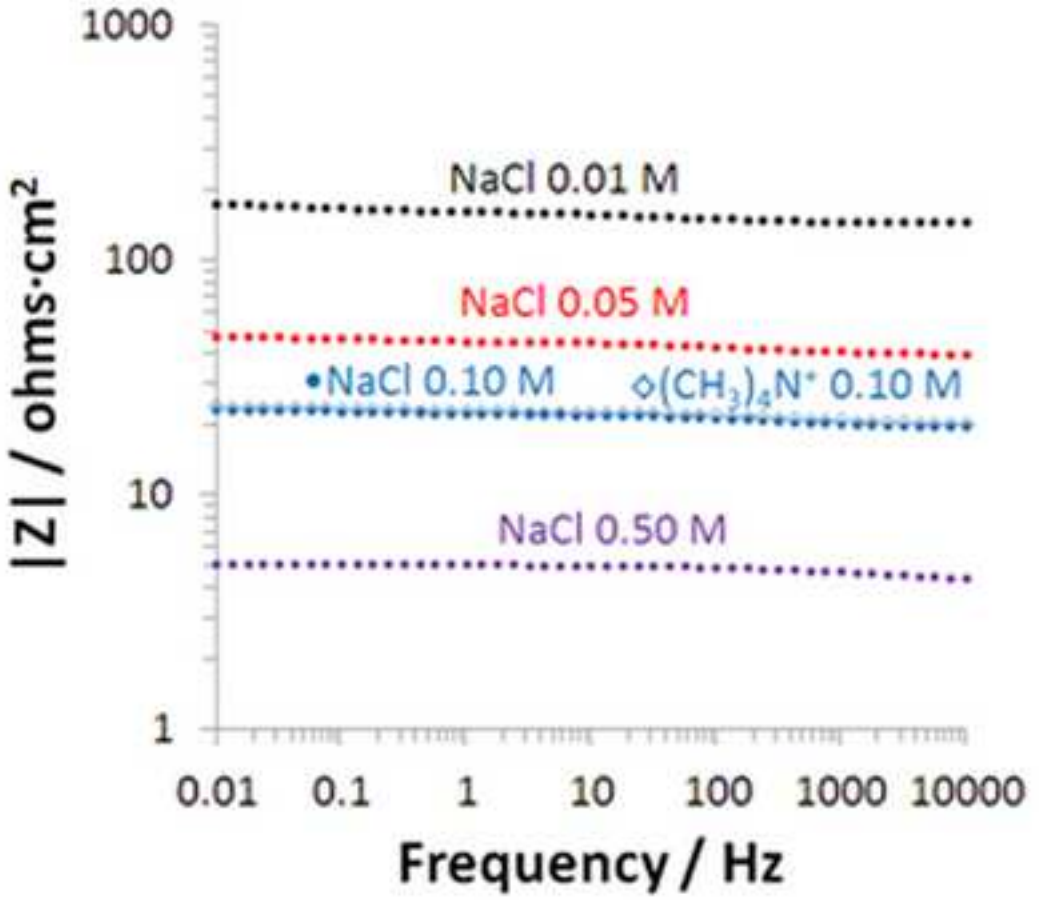

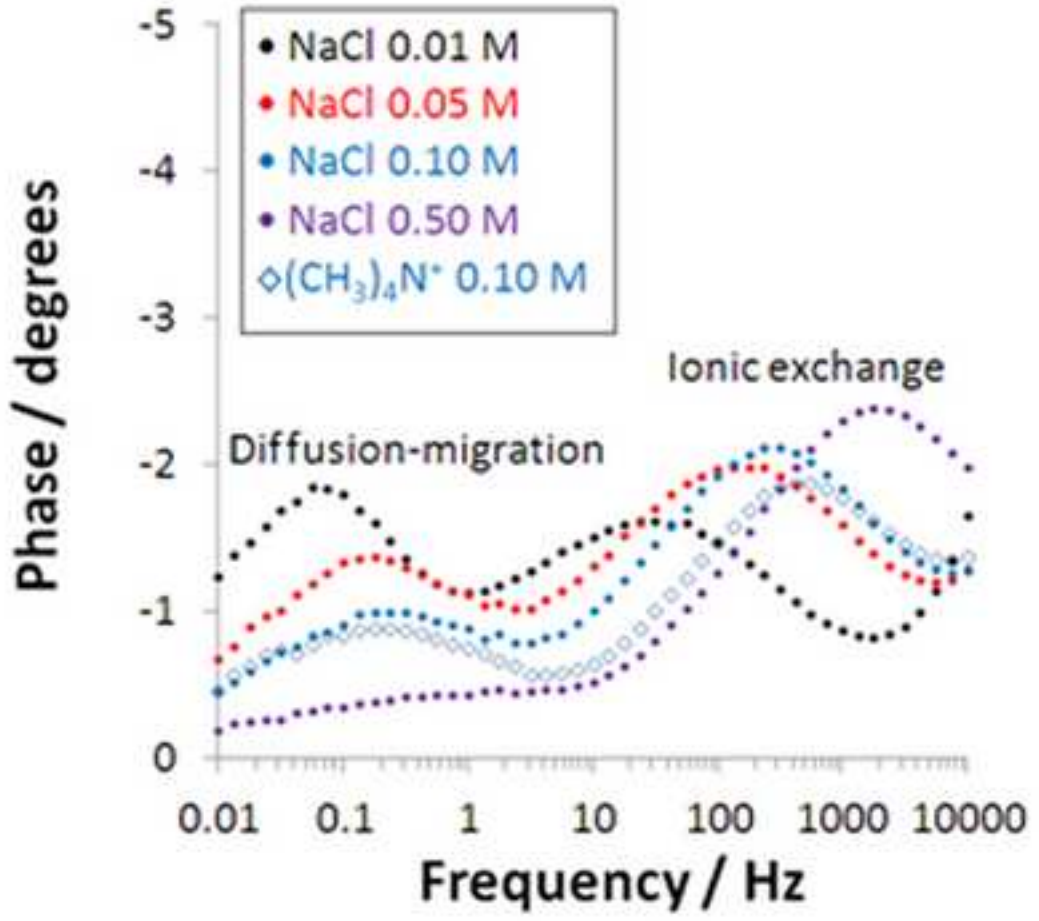

Figure 13
Click here to download high resolution image

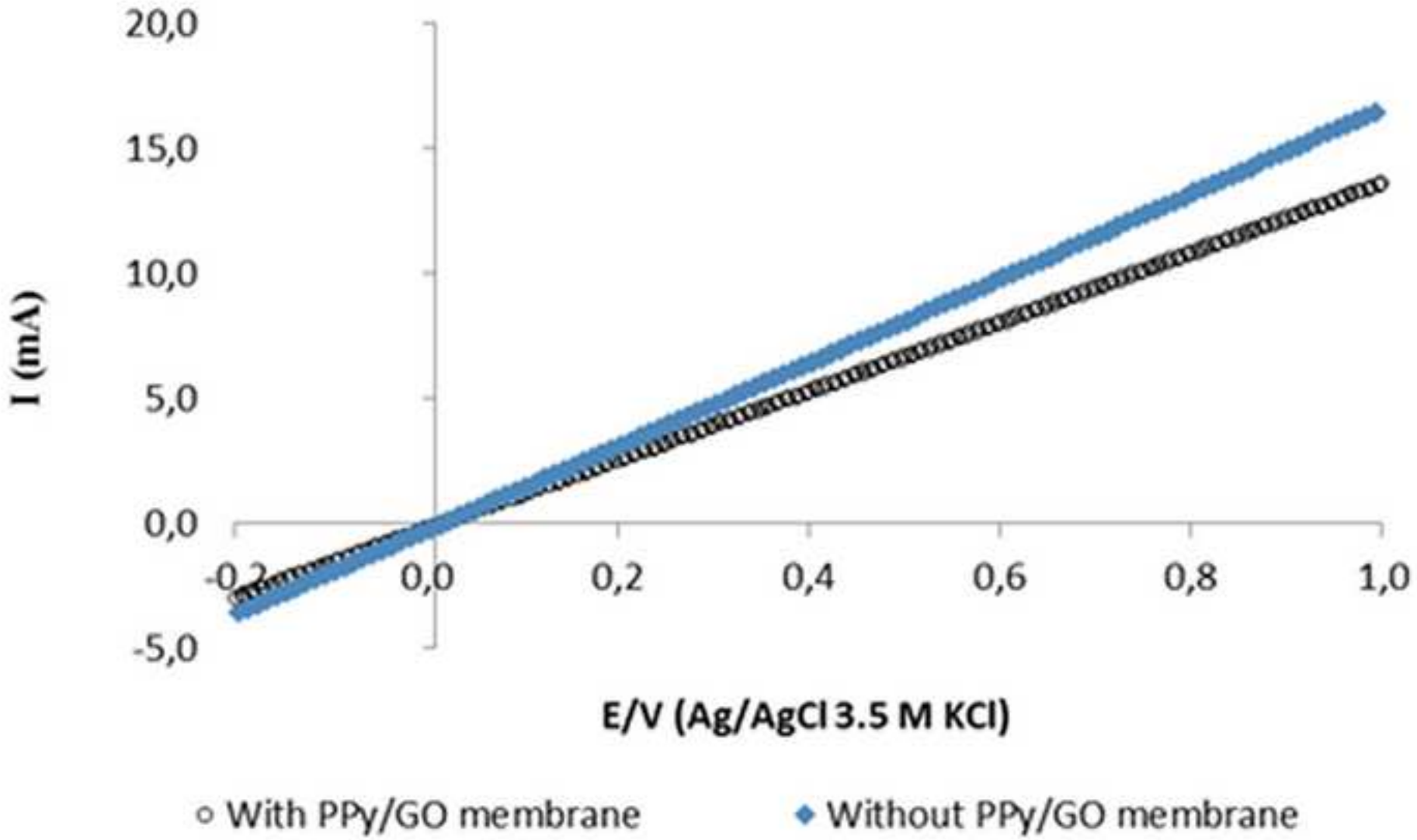

Figure 14

Click here to download high resolution image

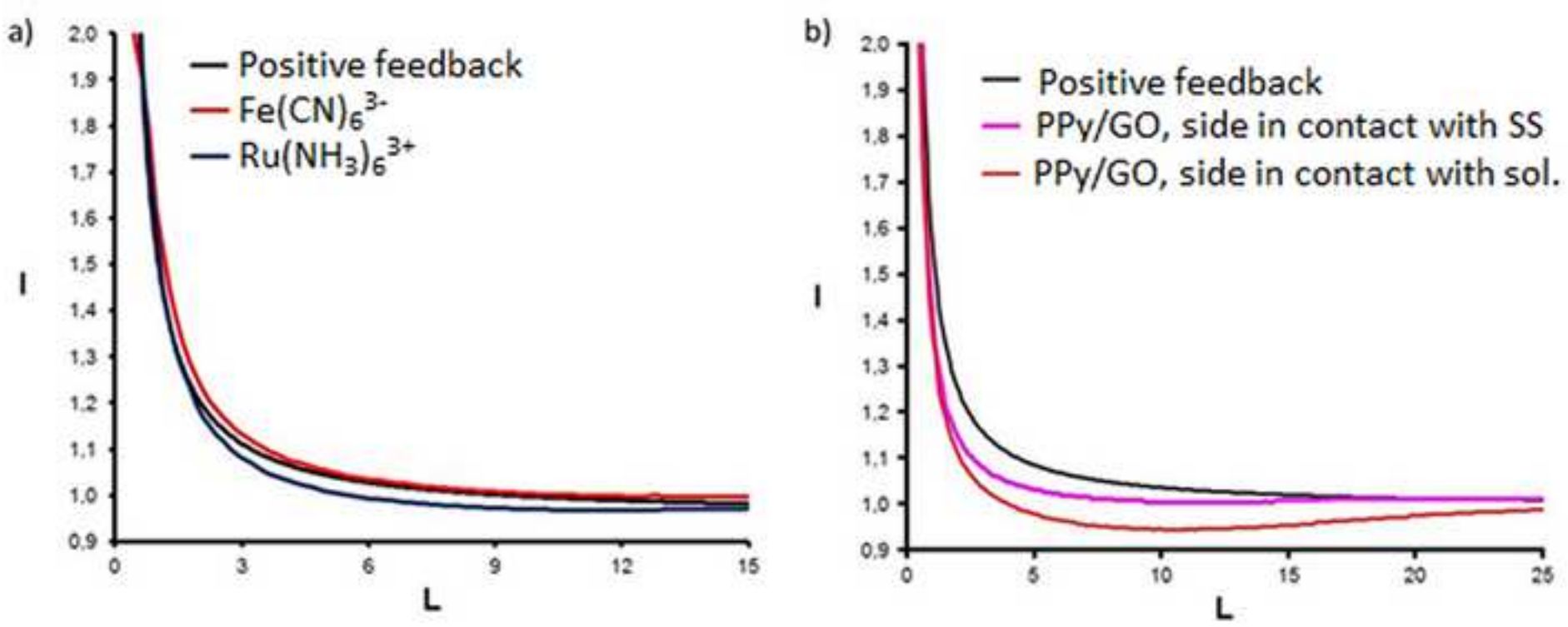

Figure 15

Click here to download high resolution image